https://doi.org/10.5194/egusphere-2024-614
Preprint. Discussion started: 5 March 2024

Technical Note: Nighttime OH and HO_2 chemical equilibria in the mesosphere – lower thermosphere

Mikhail Yu. Kulikov[1], Mikhail V. Belikovich[1], Aleksey G. Chubarov[1], Svetlana O. Dementyeva[1], and Alexander M. Feigin[1]

[1]A. V. Gaponov-Grekhov Institute of Applied Physics of the Russian Academy of Sciences, 46 Ulyanov Str., 603950 Nizhny Novgorod, Russia

Correspondence to: Mikhail Yu. Kulikov (mikhail_kulikov@mail.ru)

Abstract. At the altitudes of the mesosphere – lower thermosphere, OH and HO_2 play a significant role in many physicochemical processes. Thus, monitoring of their spatiotemporal evolution together with other chemically active trace gases is one of the most important problems for this atmosphere region, in which direct measurements are difficult. The paper studies the nighttime OH and HO_2 chemical equilibria using the 3D chemical transport modeling within the general approach including the extraction of the main sources and sinks in the equilibrium space-time areas and derivation of analytical criteria for equilibrium validity. The presented analysis shows that there are extended areas, where nighttime HO_2 and OH are close to their local equilibrium concentrations determined mainly by the reaction between HO_x – O_x components themselves and with H_2O_2, N, NO, NO_2, and CO. In the upper mesosphere – lower thermosphere, the equilibrium expressions can be shortened, including the HO_x – O_x chemistry only. These conditions describes the HO_2 and OH equilibrium from the top to the some lower borders, the altitude position of which vary in the interval between 72-73 and 85 km and depends essentially on season and latitude. The developed analytical criteria almost everywhere well reproduce the main features of these borders. The obtained results allow to extend the abilities of previously proposed methods for the retrieval of poorly measured components from measurement data and to develop new approaches.

https://doi.org/10.5194/egusphere-2024-614
Preprint. Discussion started: 5 March 2024

1 Introduction

Monitoring the spatiotemporal evolution of chemically active trace gases is one of the most important problems in atmospheric research. Despite the increase of the experimental data volume nowadays, primarily due to the development of remote sensing methods, many important trace gases continue to be unavailable for direct and regular measurements. A well-known way to increase the information content of experimental campaigns is to use chemical transport models and available experimental data for deriving unmeasured characteristics indirectly. Within the framework of this approach, the model acts as *a priori* relationship between directly measured and retrieved characteristics. The simplest model, that makes it possible to implement this approach, is based on the condition of local (in both time and space) photochemical/chemical balance (local equilibrium) between sources and sinks of the so-called "fast" components: trace gases with short lifetimes relatively, in particular, to the characteristic transport times. Mathematically, this condition does not mean that the fast variables are at equilibrium, but when it is fulfilled, the corresponding concentrations are close to their instantaneous equilibrium values. At the same time, due to the strong dissipation, in most cases (except the special cases where the ensemble of fast components includes the slow family of these components), there is no need to follow the law of matter conservation. It is possible to discard insignificant sinks and sources in the corresponding balance equations without loss of accuracy, including those caused by transport. The resulting algebraic equations are the simplest a priori local relations between measurable and retrieved trace gases. These relationships can be used to derive information about hard-to-measure atmospheric species, determine key atmospheric characteristics (for example, temperature), validate the data quality of simultaneous measurements of several atmospheric components, estimate reaction rate constants known with high uncertainty, evaluate sources (emissions), etc.

For several decades, the photochemical/chemical equilibrium approximation have been used to solve many atmospheric tasks. It is applied (see, e.g., the short review in Kulikov et al. (2018a) and references therein) in investigations of the surface layer and free troposphere chemistry in different regions (over megalopolises, in rural areas, in the mountains, over the seas), in stratospheric chemistry studies, including derivation of a critical parameters of the ozone destruction catalytic cycles, and to study the HO_x – O_x chemistry and airglows **(**$O(^1S)$ green-line, O_2 A-band, OH Meinel band emissions**)** at the heights of the mesosphere – lower thermosphere. In the latter case, the distributions of unmeasured characteristics are determined from the data of daytime and nighttime rocket and satellite measurements (e.g., Evans and Llewellyn, 1973; Good, 1976; Pendleton et al., 1983; McDade et al., 1985; McDade and Llewellyn, 1988; Evans et al., 1988; Thomas, 1990; Llewellyn et al., 1993; Llewellyn and McDade, 1996; Russell and Lowe, 2003; Russell et al., 2005; Kulikov et al., 2006, 2009, 2017, 2022a, 2022b; Mlynczak et al., 2007, 2013a, 2013b, 2014, 2018; Smith et al., 2010; Xu et al., 2012; Siskind et al., 2008, 2015;

https://doi.org/10.5194/egusphere-2024-614
Preprint. Discussion started: 5 March 2024

Fytterer et al., 2019) with the use of equilibrium assumptions for ozone and excited states of OH, O, and O_2. For example, such an approach is applied to the data of the SABER (Sounding of the Atmosphere using Broadband Emission Radiometry) instrument onboard the TIMED (Thermosphere Ionosphere Mesosphere Energetics and Dynamics) satellite, which since 2002 continues to measure simultaneous profiles of temperature, ozone, and volume emission rates of OH* transitions in wide ranges of altitude, local time, and latitude with a rather high space-time resolution.

Note a number of general aspects of the application of equilibrium conditions in the above examples. First, there are no clear criteria why the equilibrium condition should be satisfied. Usually, a certain component is taken to be a fast variable if its lifetime is much shorter than the lifetimes of other components of studied photochemical/chemical system or the duration of a day, daytime, nighttime, etc. For example, in the papers on SABER data processing (Mlynczak et al., 2013a, 2013b, 2014, 2018), it is assumed that the nighttime ozone chemical equilibrium in the mesopause is well fulfilled at altitudes of 80–100 km, since the nighttime ozone lifetime at these altitudes is too short varying in the range from several minutes to several tens of minutes. Note this assumption is quite popular and used in different tasks (e.g., Swenson and Gardner, 1998; Marsh et al., 2006; Smith et al., 2009; Nikoukar et al., 2007; Xu et al., 2010, 2012; Kowalewski et al., 2014; Grygalashvyly et al., 2014; Grygalashvyly, 2015; Sonnemann et al., 2015; Kulikov et al., 2021). Belikovich et al. (2018) and Kulikov et al. (2018b, 2019, 2023a) analyzed the nighttime ozone chemical equilibrium numerically, analytically, and with the use of SABER/TIMED data. It was revealed that the short lifetime is not a sufficient condition, so this equilibrium may be significantly disrupted above 80 km. Secondly, there is no detailed numerical examination of this approximation validity, depending on altitude, latitude, local time, and season. Correspondingly, there is no the assessment of possible errors in retrieved characteristics due to disturbance of the used equilibrium condition.

Starting since our papers by Belikovich et al. (2018) and Kulikov et al. (2018b, 2019, 2023a), we develop the general approach to correct search of fast components using the data from a global 3D chemical transport model. It includes:

1. Plotting of the equilibrium space-time maps of interested component.
2. Identification of the main sources and sinks in the found equilibrium areas.
3. Derivation and subsequent use of analytical criteria that make it possible to determine the fulfillment of the equilibrium condition locally (in time and space) with the use of the measurement data only.

The last point is based on the theory of chemical equilibrium of a certain trace gas based on estimations of its lifetime and equilibrium concentration and time dependences of these characteristics (Kulikov et al., 2023a).

https://doi.org/10.5194/egusphere-2024-614
Preprint. Discussion started: 5 March 2024

The main goals of this paper is to apply mentioned approach for analysis of nighttime OH and HO_2 chemical equilibriums in the mesosphere – lower thermosphere. Along with O and H, OH and HO_2 are important components of HO_x – O_x chemistry participating (a) in chemical heating through, in particular, $O+OH \rightarrow O_2+H$ and $O+HO_2 \rightarrow O_2+OH$ exothermic reactions, (b) in formation of airglows, (c) in catalytic cycles of the ozone destruction. Moreover, the equilibrium conditions of OH and HO_2 are additional *a priori* relationships that can be used to retrieve these components or other characteristics from measured data. In particular, the method proposed by Panka et al. (2021) for total OH retrieval from SABER/TIMED data at 80-100 km does not use the nighttime ozone chemical equilibrium, but nevertheless, applies the equilibrium between sources and sinks for all exited and ground states of OH (v=0-9). Therefore, this approach is tested in our paper.

In the next section, we present the used model and methods. In Section 3, the model data are used to plot HO_2 and OH equilibrium maps. In Sections 4-5, we extract the main reactions determining equilibria of these gases and present their shortened equilibria conditions at the upper mesosphere and lower thermosphere altitudes. In Section 6, the criteria for HO_2 and OH equilibria validity are developed. In Section 7, we discuss the obtained results and their possible applications.

2 Used 3D model and Approaches

The analysis of OH and HO_2 nighttime chemical equilibria was carried out using the data obtained with calculation of 3D chemical transport model of the middle atmosphere developed at the Leibniz Institute of Atmospheric Physics (e.g., Sonnemann et al., 1998; Körner & Sonnemann, 2001; Grygalashvyly et al., 2009; Hartogh et al., 2004, 2011) to investigate the mesosphere – lower thermosphere chemistry, in particular, in the extended mesopause region. A number of papers (e.g., Hartogh et al., 2004, 2011; Sonnemann, et al., 2006, 2008) validated the model with measurements, in particular, for ozone and water vapour.

The space-time distribution of temperature and winds were taken from the model of the dynamics of the middle atmosphere COMMA-IAP (e.g., Kremp et al., 1999; Berger and von Zahn, 1999) with an updated frequency of 1 day and linear smoothing between subsequent updates to avoid unrealistic jumps in the calculated concentrations of trace gases. 3D advective transport is taken into account with the use of the Walcek-scheme (Walcek, 2000). The vertical diffusive transport (turbulent and molecular) is calculated with the use of the implicit Thomas algorithm (Morton and Mayers, 1994). The model grid includes 118 pressure-head levels (0–135 km), 16 latitudinal and 32 longitudinal levels. The chemical module (see Table 1) comprises 25 constituents (O, $O(^1D)$, O_3, H, OH, HO_2, H_2O_2, H_2O, H_2, N, NO, NO_2, NO_3, N_2O, CH_4, CH_2, CH_3, CH_3O_2, CH_3O, CH_2O, CHO, CO, CO_2, O_2, N_2), 54 chemical reactions

https://doi.org/10.5194/egusphere-2024-614
Preprint. Discussion started: 5 March 2024

between them, and 15 photo-dissociation reactions. The model utilizes the pre-calculated dissociation rates (Kremp et al., 1999) and their dependence on the altitude and solar zenith angle.

The model was used to calculate a one-year global evolution of the above mentioned trace gases. For removing the transition regions corresponding to sunset and sunrise, we took into account the local time when the solar zenith angle > 95°. As a result, we find the spatiotemporal series of the OH/OH^{eq} and $HO_2/{HO_2}^{eq}$ ratios. Here, OH and HO_2 are the local nighttime values of hydroxyl and hydroperoxy radicals calculated by the model, OH^{eq} and ${HO_2}^{eq}$ are their local equilibrium values corresponding to the instantaneous balance between production and loss terms, respectively. Therefore, for determination of each local value of OH^{eq} and ${HO_2}^{eq}$, we used the local values of the parameters (temperature, O_2, and N_2) and the concentrations of other trace gases determining local chemical sources and sinks of OH and HO_2. Then, the OH/OH^{eq} and $HO_2/{HO_2}^{eq}$ series were averaged over the zonal coordinate and time during each month and were presented as height-latitude maps, depending on the month. Each map contains lines marking the boundaries of the equilibrium areas, where the following conditions are satisfied:

$$\begin{cases} |< OH/OH^{eq} > -1| \le 0.1 \\ \sigma_{OH/OH^{eq}} \le 0.1 \end{cases}, \begin{cases} |< HO_2/{HO_2}^{eq} > -1| \le 0.1 \\ \sigma_{HO_2/{HO_2}^{eq}} \le 0.1 \end{cases}, \quad (1)$$

where the angle brackets are used to denote the values averaged in time and space, $\sigma_{OH/OH^{eq}}$ and $\sigma_{HO_2/{HO_2}^{eq}}$ are standard deviations of the OH/OH^{eq} and $HO_2/{HO_2}^{eq}$ ratios from 1, respectively.

Then, we plotted spatiotemporal maps showing the relative contribution of each reaction to a summarized source or sink at all altitudes and latitudes. These maps helped us to identify the main sources and sinks describing the chemical equilibrium of nighttime OH and HO_2 in the equilibrium areas to an accuracy of better than a few percent.

At final stage, we obtained and verified the analytical criteria of OH and HO_2 nighttime chemical equilibria according to Kulikov et al. (2023a). The paper considered the poorly chemical evolution of a certain trace gas n. It was shown strictly mathematically, that the local values of n and its equilibrium concentration n^{eq} are close to each other ($n(t) \approx n^{eq}(t)$), when $\tau_n \ll \tau_{n^{eq}}$, where τ_n is the n lifetime and $\tau_{n^{eq}}$ is the local time scale of n^{eq}:

$$\tau_{n^{eq}} \equiv \frac{n^{eq}}{|dn^{eq}/dt|}. \quad (2)$$

The expression for τ_n is found from total sink of n. The expression for $\tau_{n^{eq}}$ is derived with the use of differential equations describing chemical evolution of other reacting components which determine the expression for n^{eq}. Kulikov et al. (2023a) also showed the criterion

https://doi.org/10.5194/egusphere-2024-614
Preprint. Discussion started: 5 March 2024

$$\tau_n/\tau_{n^{eq}} \leq 0.1 \quad (3)$$

is sufficient, in order to the possible difference between n and n^{eq} to be no more than 0.1.

3 Nighttime HO_2 and OH chemical equilibriums

According to the Table 1, HO_2 chemical sources in nighttime are determined by the following reactions:

H+O_2+M → HO_2+M (R20), OH+O_3 → O_2+HO_2 (R22), H_2O_2+OH → H_2O+HO_2 (R29), H_2O_2+O → OH+HO_2 (R19), CHO+O_2 → HO_2+CO (R40), CH_3O+O_2 → CH_2O+HO_2 (R37),

whereas chemical sinks of this component are as follows:

HO_2+O → OH+O_2 (R18), HO_2+O_3 → OH+2O_2 (R23), OH+HO_2 → H_2O+O_2 (R28), H+HO_2 → 2OH (R14), H+HO_2 → H_2O+O (R15), H+HO_2 → H_2+O_2 (R16), NO+HO_2 → NO_2+OH (R50), HO_2+HO_2 → H_2O_2+O_2 (R30), HO_2+HO_2+M → H_2O_2+O_2+M (R31).

Thus, HO_2 local equilibrium concentration is described by the following equation:

$$HO_2{}^{eq} = \frac{k_{20}\cdot H\cdot M\cdot O_2 + k_{22}\cdot OH\cdot O_3 + k_{29}\cdot H_2O_2\cdot OH + k_{19}\cdot H_2O_2\cdot O + k_{40}\cdot CHO\cdot O_2 + k_{37}\cdot CH_3O\cdot O_2}{k_{18}\cdot O + k_{23}\cdot O_3 + k_{28}\cdot OH + (k_{14}+k_{15}+k_{16})\cdot H + k_{50}\cdot NO + 2\cdot(k_{30}+k_{31}\cdot M)\cdot HO_2} \quad (4)$$

The Figure 1 plots height-latitude cross sections for the $< HO_2/HO_2{}^{eq} >$ ratio for each month. The dashed area corresponds to χ<95°. The white area represents the ratio outside the [0.5, 1.5] interval. The black solid lines mark the borders of equilibrium areas, where, according to (1), local values of HO_2 are close to their equilibrium values with a possible bias of less than 10%. At low and middle latitudes, one can see the present of the main equilibrium area, which extends from the top of the analyzed altitude range to the lower boundary. The height of this equilibrium border, $z_{HO_2^{eq}}$, depends on the season and latitude and varies in the interval between 73 and 85 km. It is the highest and the lowest during the summer and winter respectively at the middle latitudes. Near equator, $z_{HO_2^{eq}}$ demonstrates the weakest annual variations and varies in the range of 81-83 km. There are local areas below the upper longest black line, but they are small and irregular and can be omitted from our consideration. Note only that the maps in many months show the existence of equilibrium near 50 km, which can be assumed to be the beginning of the main equilibrium area in the stratosphere. At high latitudes, there is the main equilibrium area as at low and middle latitudes, but this area above 70-75° of latitude can extend down to 50 km with small exceptions.

In accordance to the Table 1, OH chemical sources are determined by the following reactions:

https://doi.org/10.5194/egusphere-2024-614
Preprint. Discussion started: 5 March 2024

$H+O_3 \rightarrow OH+O_2$ (R21), $HO_2+O \rightarrow OH+O_2$ (R18), $HO_2+O_3 \rightarrow OH+2O_2$ (R23), $H+HO_2 \rightarrow 2OH$ (R14), $NO+HO_2 \rightarrow NO_2+OH$ (R50), $H_2O_2+O \rightarrow OH+HO_2$ (R19), $H+NO_2 \rightarrow OH+NO$ (R51), $O(^1D)+H_2O \rightarrow 2OH$ (R7), $O(^1D)+H_2 \rightarrow H+OH$ (R8), $CH_4+O(^1D) \rightarrow CH_3+OH$ (R9),

whereas chemical sinks of this component are as follows:

$OH+O \rightarrow H+O_2$ (R17), $OH+O_3 \rightarrow O_2+HO_2$ (R22), $OH+HO_2 \rightarrow H_2O+O_2$ (R28), $OH+OH \rightarrow H_2O+O$ (R26), $OH+OH+M \rightarrow H_2O_2+M$ (R27), $H+OH+N_2 \rightarrow H_2O+N_2$ (R24), $H_2O_2+OH \rightarrow H_2O+HO_2$ (R29), $OH+CO \rightarrow H+CO_2$ (R32), $CH_4+OH \rightarrow CH_3+H_2O$ (R33), $OH+H_2 \rightarrow H_2O+H$ (R25), $N+OH \rightarrow NO+H$ (R49).

Thus, OH local equilibrium concentration is described by the following equation:

$$OH^{eq} = (k_{21} \cdot H \cdot O_3 + k_{18} \cdot O \cdot HO_2 + k_{23} \cdot HO_2 \cdot O_3 + 2 \cdot k_{14} \cdot H \cdot HO_2 + k_{50} \cdot HO_2 \cdot NO + k_{19} \cdot H_2O_2 \cdot O + k_{24} \cdot H \cdot N_2 + k_{51} \cdot NO_2 \cdot H + 2 \cdot k_7 \cdot O(^1D) \cdot H_2O + k_8 \cdot O(^1D) \cdot H_2 + k_9 \cdot O(^1D) \cdot CH_4) / (k_{17} \cdot O + k_{22} \cdot O_3 + k_{28} \cdot HO_2 + 2 \cdot (k_{26} + k_{27} \cdot M) \cdot OH + k_{29} \cdot H_2O_2 + k_{32} \cdot CO + k_{33} \cdot CH_4 + k_{25} \cdot H_2 + k_{25} \cdot N) \quad (5)$$

Figure 2 shows height-latitude cross sections for the $< OH/OH^{eq} >$ ratio for each month. In this case, the equilibrium covers up to 70-80% of the presented ranges of heights and latitudes, so that the black solid lines mark the external borders of non-equilibrium areas. In March and September, this area is almost symmetrical to the equator. In April-August, it is shifted towards the northern hemisphere. In October-February, this area is higher in the southern hemisphere. In all months, it is below 85-86 km. In the polar regions, there are latitudinal ranges where OH is close to equilibrium throughout the entire range of heights.

4 The main reactions determining HO_2 and OH equilibriums

The Figure 3 shows height-latitude contour maps showing the relative contribution of a certain reaction to the total source of HO_2 in different months taken for example. To increase the information content of the panels, the altitude range is cut off everywhere to 100 km, since there are no significant changes above. Note, first, that reaction $H+O_2+M \rightarrow HO_2+M$ determines a major (up to 95% and more) contribution in the main equilibrium area almost everywhere except for the polar regions above 70-75° of latitude and below 75-80 km, where the reactions $OH+O_3 \rightarrow O_2+HO_2$ and $H_2O_2+OH \rightarrow H_2O+HO_2$ become important and should be taken into account. Second, other reactions ($H_2O_2+O \rightarrow OH+HO_2$, $CHO+O_2 \rightarrow HO_2+CO$, $CH_3O+O_2 \rightarrow CH_2O+HO_2$) together contribute less than 2-3% to the total source of HO_2 in the main equilibrium area and may be omitted.

https://doi.org/10.5194/egusphere-2024-614
Preprint. Discussion started: 5 March 2024

The Figure 4 presents height-latitude contour maps showing the relative contribution of a certain reaction to the total sink of HO_2 in the same months as in Figure 3. Firstly, it should be noted that reaction $HO_2+O \rightarrow OH+O_2$ determines a major (up to 95% and more) contribution in the main equilibrium area almost everywhere except for the same small polar areas, as in the considered case with the sources, where the reactions $HO_2+O_3 \rightarrow OH+2O_2$ and $NO+HO_2 \rightarrow NO_2+OH$ are important and should be taken into account. Secondly, the reactions $OH+HO_2 \rightarrow H_2O+O_2$, $H+HO_2 \rightarrow 2OH$, $H+HO_2 \rightarrow H_2O+O$, and $H+HO_2 \rightarrow H_2+O_2$ give together contribute up to 10-15% of the total source near the boundary of the main equilibrium area. Thirdly, the remaining reactions ($HO_2+HO_2 \rightarrow H_2O_2+O_2$, $HO_2+HO_2+M \rightarrow H_2O_2+O_2+M$) are not important in the main equilibrium area and can be omitted.

Therefore, the expression for HO_2 local equilibrium concentration can be simplified as follows:

$$HO_2^{eq} = \frac{k_{20}\cdot H\cdot M\cdot O_2+k_{22}\cdot OH\cdot O_3+k_{29}\cdot H_2O_2\cdot OH}{k_{18}\cdot O+k_{23}\cdot O_3+k_{28}\cdot OH+(k_{14}+k_{15}+k_{16})\cdot H+k_{50}\cdot NO} \quad (6)$$

Figures 5-6 show height-latitude contour maps showing the relative contribution of a certain reaction to the total source of OH in the same months as in Figure 3 taken for example. As in the previous case, the altitude range is cut off at 100 km, because only the panels for the reactions $H+O_3 \rightarrow OH+O_2$ and $HO_2+O \rightarrow OH+O_2$ consist of interesting variations at the 100-130 km altitudes. Note that these reactions are the main OH sources in the upper part of the presented distributions down to 70-75 km, where they jointly provide up to 95% contribution in equilibrium concentration. Also, the reaction $HO_2+O_3 \rightarrow OH+2O_2$ is major in the lower part of the presented distributions from 50 to 60-70 km, depending on the month. The reaction $NO+HO_2 \rightarrow NO_2+OH$ is important around non-equilibrium areas of OH and should be taken into account, whereas the reaction $H+NO_2 \rightarrow OH+NO$ is important in compact altitude-latitude areas near the poles, the reaction $H+HO_2 \rightarrow 2OH$ gives up to 10-15% contribution in small areas near the equilibrium boundary. Other reactions ($O(^1D)+H_2O \rightarrow 2OH$, $O(^1D)+H_2 \rightarrow H+OH$, $CH_4+O(^1D) \rightarrow CH_3+OH$, $H_2O_2+O \rightarrow OH+HO_2$) together contribute less than 2-3% of the total source of OH in the main equilibrium area and can be omitted.

Figures 7-8 present height-latitude contour maps showing the relative contribution of a certain reaction to the total sink of OH. First, note that the reaction $OH+O \rightarrow H+O_2$ is the main OH sink in the upper part of the presented distributions down to 70-80 km, depending on the month, where it provides up to 95% of the equilibrium concentration. The reactions $OH+CO \rightarrow H+CO_2$ and $OH+O_3 \rightarrow O_2+HO_2$ are major in the lover part of the presented distributions from 50 to 70-80 km, depending on the month. The reaction $OH+HO_2 \rightarrow H_2O+O_2$ is remarkable around non-equilibrium areas of OH, whereas the reaction $H_2O_2+OH \rightarrow H_2O+HO_2$ is important in the compact altitude-latitude area near the poles. Other reactions ($OH+OH \rightarrow H_2O+O$, $OH+H_2 \rightarrow H_2O+H$, $N+OH \rightarrow NO+H$, $CH_4+OH \rightarrow CH_3+H_2O$, $H+OH+N_2 \rightarrow$

https://doi.org/10.5194/egusphere-2024-614
Preprint. Discussion started: 5 March 2024

H_2O+N_2, $OH+OH+M \rightarrow H_2O_2+M$) together contribute less than 2-3% to the total source of OH in the main equilibrium area and can be omitted.

Therefore, the expression for OH local equilibrium concentration can be can be simplified as follows:

$$OH^{eq} = \frac{k_{21}\cdot H\cdot O_3+k_{18}\cdot O\cdot HO_2+k_{23}\cdot HO_2\cdot O_3+2\cdot k_{14}\cdot H\cdot HO_2+k_{24}\cdot H\cdot N_2+k_{50}\cdot HO_2\cdot NO+k_{51}\cdot NO_2\cdot H}{k_{17}\cdot O+k_{22}\cdot O_3+k_{28}\cdot HO_2+k_{29}\cdot H_2O_2+k_{32}\cdot CO} \quad (7)$$

5 Shortened equilibrium conditions of HO_2 and OH in the upper mesosphere and lower thermosphere

The above analysis revealed that the reactions describing the equilibrium conditions (6-7) in the lower and middle mesosphere are mainly different from those in the upper mesosphere and lower thermosphere. This means that the task of applying these conditions can be divided into two parts depending on the selected altitude range. At the upper mesosphere and lower thermosphere altitudes, we can consider only the $HO_x - O_x$ chemistry, excluding the reactions with participation of H_2O_2, N, NO, NO_2, and CO. In addition, we can omit the reactions $HO_2+O_3 \rightarrow OH+2O_2$, $OH+O_3 \rightarrow O_2+HO_2$, and $OH+HO_2 \rightarrow H_2O+O_2$ due to their insignificance here. As the result, the shortened equilibrium conditions of HO_2 and OH for this altitude range are as follows:

$$HO_{2_{sh}}^{eq} = \frac{k_{20}\cdot H\cdot M\cdot O_2}{k_{18}\cdot O+(k_{14}+k_{15}+k_{16})\cdot H}, \quad (8)$$

$$OH_{sh}^{eq} = \frac{k_{21}\cdot H\cdot O_3+k_{18}\cdot O\cdot HO_2+2\cdot k_{14}\cdot H\cdot HO_2}{k_{17}\cdot O} \quad (9)$$

The Figure 9 shows height-latitude cross sections for the $< HO_2/HO_{2_{sh}}^{eq} >$ ratio for each month. In each panel, the upper longest black line marks the lower border of the main equilibrium area, where, according to (1), $HO_2 \approx HO_{2_{sh}}^{eq}$ with possible bias of less than 10%. As in the case of Figure 1, this area extends from the top of the analyzed altitude range. There are also very small equilibrium areas below, which can be omitted from our consideration. The height of the lower border of the main equilibrium area, $z_{HO_{2_{sh}}^{eq}}$, depends essentially on the season and latitude. Comparing with Figure 1, one can see, it repeats well many features of $z_{HO_{2_{sh}}^{eq}}$ at low and middle latitudes. In particular, $z_{HO_{2_{sh}}^{eq}}$ varies in the interval between 73 and 85 km, as in the case of $z_{HO_2^{eq}}$. In the middle latitudes, $z_{HO_{2_{sh}}^{eq}}$ in summer is several km higher than in winter. Near equator, $z_{HO_{2_{sh}}^{eq}}$ demonstrates the weakest annual variations and varies in the range of 81-83 km. So, one can conclude that the exclusion of a number of reactions does not lead to significant changes in the space-time distributions of the HO_2 equilibrium.

https://doi.org/10.5194/egusphere-2024-614
Preprint. Discussion started: 5 March 2024

The Figure 10 plots height-latitude cross sections for the $< OH/OH_{sh}^{eq} >$ ratio for each month. As in the previous case, this is the lower border of the equilibrium area, where, according to (1), $OH \approx OH_{sh}^{eq}$ with good precision. The dependence of the border height, $z_{OH_{sh}^{eq}}$, on the season and latitude repeats mainly $z_{HO_{2_{sh}}^{eq}}$. In particular, $z_{OH_{sh}^{eq}}$ varies in the interval between 73 and 85 km. At middle latitudes, $z_{OH_{sh}^{eq}}$ in summer is several km higher than in winter. Near the equator, $z_{OH_{sh}^{eq}}$ also demonstrates the weakest annual variations and varies in the range of 81-83 km. Nevertheless, in some cases, the OH equilibrium border lies slightly higher than the HO_2 border. In particular, it can be seen in April-August above 50ºS, which can be explained by the difference between HO_2 and OH lifetimes ($\tau_{HO_2} < \tau_{OH}$), mainly, due to $k_{18} > k_{17}$. Comparing with Figure 2, one can see that the exclusion of the mentioned reactions from consideration results in the absence of the OH equilibrium areas at the low and middle mesosphere altitudes, as expected.

6 The criterions for HO_2 and OH equilibrium validity in the upper mesosphere and lower thermosphere

Let determine HO_2 and OH lifetimes and the local time scales of $HO_{2_{sh}}^{eq}$ and OH_{sh}^{eq}, according to Section 2.

From (8), HO_2 lifetime and the local time scales of $HO_{2_{sh}}^{eq}$ are as follows:

$$\tau_{HO_2} = \frac{1}{k_{18}\cdot O+(k_{14}+k_{15}+k_{16})\cdot H}, \quad (10)$$

$$\tau_{HO_{2_{sh}}^{eq}} = \frac{HO_{2_{sh}}^{eq}}{|dHO_{2_{sh}}^{eq}/dt|}. \quad (11)$$

Let find the expression for $dHO_{2_{sh}}^{eq}/dt$:

$$\frac{dHO_{2_{sh}}^{eq}}{dt} = \frac{k_{18}\cdot k_{20}\cdot M\cdot O_2\cdot\frac{d}{dt}(\frac{H}{O})\cdot O^2}{(k_{18}\cdot O+(k_{14}+k_{15}+k_{16})\cdot H)^2} = -\frac{k_{18}\cdot k_{20}\cdot M\cdot O_2\cdot\frac{d}{dt}(\frac{O}{H})\cdot H^2}{(k_{18}\cdot O+(k_{14}+k_{15}+k_{16})\cdot H)^2}. \quad (12)$$

Kulikov et al. (2023a) analyzed analytically the local nighttime evolution of O and H within the framework of pure HO_x – O_x chemistry and found the expression for $\frac{d}{dt}(\frac{O}{H})$:

$$\frac{d}{dt}\left(\frac{O}{H}\right) = -2\cdot k_{20}\cdot M\cdot O_2\cdot\left(1-\frac{k_{15}+k_{16}}{k_{18}}\right) - k_{21}\cdot O_3 - k_{12}\cdot M\cdot O_2\cdot\frac{O}{H}. \quad (13)$$

Thus, the expression (12) can be rewritten in following form:

$$\frac{dHO_{2_{sh}}^{eq}}{dt} = \frac{k_{18}\cdot k_{20}\cdot M\cdot O_2\cdot H^2\cdot(2\cdot k_{20}\cdot M\cdot O_2\cdot\left(1-\frac{k_{15}+k_{16}}{k_{18}}\right)+k_{21}\cdot O_3+k_{12}\cdot M\cdot O_2\cdot\frac{O}{H})}{(k_{18}\cdot O+(k_{14}+k_{15}+k_{16})\cdot H)^2}. \quad (14)$$

https://doi.org/10.5194/egusphere-2024-614
Preprint. Discussion started: 5 March 2024

By combining (8), (11), and (14) we obtain the expression for the local time scales of $HO_{2_{sh}}^{eq}$:

$$\tau_{HO_{2_{sh}}^{eq}} = \frac{(k_{18}\cdot O+(k_{14}+k_{15}+k_{16})\cdot H)}{k_{18}\cdot H\cdot(2\cdot k_{20}\cdot M\cdot O_2\cdot\left(1-\frac{k_{15}+k_{16}}{k_{18}}\right)+k_{21}\cdot O_3+k_{12}\cdot M\cdot O_2\cdot\frac{O}{H})} \quad (15)$$

Thus, taking into account (3), (10) and (15), the criterion for HO_2 equilibrium validity is written in the form:

$$Crit_{HO_2} = \frac{\tau_{HO_2}}{\tau_{\tau_{HO_{2_{sh}}^{eq}}}} = \frac{k_{18}\cdot H\cdot(2\cdot k_{20}\cdot M\cdot O_2\cdot\left(1-\frac{k_{15}+k_{16}}{k_{18}}\right)+k_{21}\cdot O_3+k_{12}\cdot M\cdot O_2\cdot\frac{O}{H})}{(k_{18}\cdot O+(k_{14}+k_{15}+k_{16})\cdot H)^2} \leq 0.1. \quad (16)$$

We calculated $Crit_{HO_2}$ using the global 3D chemical transport model and included the zonally and monthly averaged lines $< Crit_{HO_2} >= 0.1$ in Figure 9 (see magenta lines). One can see that, depending on the month, each red line well reproduces the lower border of the main OH equilibrium area and repeats almost all its features and variations. Note that, in zero approximation, the criterion (16) can be simplified as

$$Crit_{HO_2} \approx \left(2\cdot k_{20}\cdot M\cdot O_2\cdot\left(1-\frac{k_{15}+k_{16}}{k_{18}}\right)+k_{21}\cdot O_3+k_{12}\cdot M\cdot O_2\cdot\frac{O}{H}\right)\cdot\frac{H}{k_{18}\cdot O^2}\cdot\leq 0.1. \quad (17)$$

From (9), OH lifetime and the local time scales of OH_{sh}^{eq} are as follows:

$$\tau_{OH} = \frac{1}{k_{17}\cdot O}, \quad (18)$$

$$\tau_{OH_{sh}^{eq}} = \frac{OH_{sh}^{eq}}{|dOH_{sh}^{eq}/dt|}. \quad (19)$$

Before determining the expression for dOH_{sh}^{eq}/dt, first of all, one should to keep in mind that the expression (9) depends on the HO_2 concentration. Above mentioned, that near and above the OH equilibrium border, HO_2 is in equilibrium ($HO_2 \approx HO_{2_{sh}}^{eq}$) and we can use expression (8). In view of $k_{18}\cdot O \gg (k_{14}+k_{15}+k_{16})\cdot H$,

$$HO_{2_{sh}}^{eq} \approx \frac{k_{20}\cdot H\cdot M\cdot O_2}{k_{18}\cdot O}\left(1-\frac{(k_{14}+k_{15}+k_{16})\cdot H}{k_{18}\cdot O}\right). \quad (20)$$

The substitution of (20) into (9) yields:

$$OH_{sh}^{eq} = k_{20}\cdot H\cdot M\cdot O_2\cdot\frac{(1+\frac{2\cdot k_{14}\cdot H}{k_{18}\cdot O})\cdot(1-\frac{(k_{14}+k_{15}+k_{16})\cdot H}{k_{18}\cdot O})}{k_{17}\cdot O}+\frac{k_{21}\cdot H\cdot O_3}{k_{17}\cdot O}\approx\frac{k_{20}\cdot H\cdot M\cdot O_2}{k_{17}\cdot O}\cdot\left(1+\frac{(k_{14}-k_{15}-k_{16})\cdot H}{k_{18}\cdot O}\right)+$$
$$\frac{k_{21}\cdot H\cdot O_3}{k_{17}\cdot O} \quad (21)$$

Thus, the expression for dOH_{sh}^{eq}/dt is:

$$\frac{dOH_{sh}^{eq}}{dt} = \frac{d}{dt}\left(\frac{H}{O}\right)\cdot\left(\frac{k_{20}\cdot M\cdot O_2}{k_{17}}\cdot\left(1+\frac{2\cdot(k_{14}-k_{15}-k_{16})\cdot H}{k_{18}\cdot O}\right)+\frac{k_{21}\cdot O_3}{k_{17}}\right)+\frac{k_{21}\cdot H\cdot}{k_{17}\cdot O}\frac{dO_3}{dt}. \quad (22)$$

https://doi.org/10.5194/egusphere-2024-614
Preprint. Discussion started: 5 March 2024

Taking into account (13) and the differential equation for O_3 time evolution:

$$\frac{dO_3}{dt} = k_{12} \cdot M \cdot O_2 \cdot O - k_{21} \cdot H \cdot O_3,$$

the expression (21) can be rewritten in following form:

$$\frac{dOH_{sh}^{eq}}{dt} =$$

$$(2 \cdot k_{20} \cdot M \cdot O_2 \cdot \left(1 - \frac{k_{15}+k_{16}}{k_{18}}\right) + k_{21} \cdot O_3 + k_{12} \cdot M \cdot O_2 \cdot \frac{O}{H}) \cdot \frac{H^2}{O^2}\left(\frac{k_{20} \cdot M \cdot O_2}{k_{17}} \cdot \left(1 + \frac{2 \cdot (k_{14} - k_{15} - k_{16}) \cdot H}{k_{18} \cdot O}\right) +$$

$$k21 \cdot O3 k17 + k21 \cdot H \cdot (k12 \cdot M \cdot O2 \cdot O - k21 \cdot H \cdot O3) k17 \cdot O. \quad (23)$$

Thus, by combining (3), (18), (19), (21), and (23) we obtain the expression for the criterion for OH equilibrium validity:

$$Crit_{OH} = \frac{\tau_{OH}}{\tau_{\tau_{OH_{sh}^{eq}}}} = \frac{1}{k_{17} \cdot O} \cdot \left(\left(2 \cdot k_{20} \cdot M \cdot O_2 \cdot \left(1 - \frac{k_{15}+k_{16}}{k_{18}}\right) + k_{21} \cdot O_3 + k_{12} \cdot M \cdot O_2 \cdot \frac{O}{H}\right) \cdot \frac{H}{O} \cdot \right.$$

$$k20 \cdot M \cdot O2 \cdot 1 + 2 \cdot k14 - k15 - k16 \cdot Hk18 \cdot O + k21 \cdot O3 + k21 \cdot k12 \cdot M \cdot O2 \cdot O - k21 \cdot H \cdot O3 / (k20 \cdot M \cdot O2 \cdot (1 + k14 - k15 - k16 \cdot Hk18 \cdot O) + k21 \cdot$$

$$\left. O_3\right) \leq 0.1. \quad (24)$$

We calculated $Crit_{OH}$ using the global 3D chemical transport model and included the zonally and monthly averaged lines $< Crit_{OH} >= 0.1$ in Figure 10 (see magenta lines). One can see that, depending on the month, red line almost everywhere reproduces the lower border of the OH equilibrium area and repeats mainly its features and variations. Nevertheless, there are a few (by latitude) narrow areas (in April-August near 70ºS and in October-December near 70ºN) where the criterion gives a few km lower position of the OH equilibrium boundary, that is going to be discussed below. Note our numerical analysis shows that, in zero approximation, the criterion (24) can be simplified as:

$$Crit_{OH} \approx \left(2 \cdot k_{20} \cdot M \cdot O_2 \cdot \left(1 - \frac{k_{15}+k_{16}}{k_{18}}\right) + k_{21} \cdot O_3 + k_{12} \cdot M \cdot O_2 \cdot \frac{O}{H}\right) \cdot \frac{H}{k_{17} \cdot O^2} \cdot \leq 0.1. \quad (25)$$

7 Discussion

Let's discuss obtained results and their possible applications.

As noted, Figures 9-10 present an interesting peculiarity. At middle latitudes, summer $z_{HO_{2_{sh}}^{eq}}$ and $z_{OH_{sh}^{eq}}$ are several km higher than winter ones. Recently (Kulikov et al., 2023b) such a feature was found in the evolution of nighttime ozone chemical equilibrium boundary derived from SABER/TIMED data, whichwas accompanied by the same variation of the transition zone dividing deep and weak

https://doi.org/10.5194/egusphere-2024-614
Preprint. Discussion started: 5 March 2024

photochemical oscillations of O and H caused by the diurnal variations of solar radiation. Kulikov et al. (2023b) analyzed this effect analytically and explained by the markedly lower values of the O and H nighttime evolution times in summer than in winter by virtue, mainly, of the lower values of the O/H ratio during the night, which, in turn, is determined by the daytime photochemistry. At middle, the ozone boundary varies within 4-5 km interval above 80 km, whereas the range of OH and HO_2 boundaries variations is 72-85 km (see Figures 9-10). In the case of ozone, its criterion for equilibrium validity (see (5) in Kulikov et al. (2023b)) is as follows:

$$Crit_{O_3} = 2\frac{k_{12}\cdot O_2\cdot M}{k_{21}}(k_{20}\cdot M\cdot O_2\cdot\left(1-\frac{k_{15}+k_{16}}{k_{18}}\right)+k_{21}\cdot O_3)\cdot\frac{1}{k_{21}\cdot H\cdot O_3}\leq 0.1. \quad (26)$$

At $O_3 \approx {O_3}^{eq} = \frac{k_{12}\cdot M\cdot O_2\cdot O}{k_{21}\cdot H}$, one can see that $Crit_{O_3}\sim\frac{1}{O}$. It is follows from simplified expressions (17) and (25) that $Crit_{HO_2}$ and $Crit_{OH}$ are proportional to $\frac{H}{O^2}$. Such dependence leads to a stronger annual variation of OH and HO_2 equilibrium boundaries than in the case of O_3.

As noted, there are a few narrow areas near 70ºS,N (Figure 10) where the criterion (25) does not agree well with the OH equilibrium boundary. Our analysis revealed that the main reason is neglecting the reaction OH+CO → H+CO_2 as the source of H in the corresponding differential equation of its chemical balance. In order to improve the criterion, we revised the derivation of expression (17) for $\frac{d}{dt}\left(\frac{O}{H}\right)$ following to Kulikov et al. (2023a):

$$\frac{d}{dt}\left(\frac{O}{H}\right) = -2\cdot k_{20}\cdot M\cdot O_2\cdot\left(1-\frac{k_{15}+k_{16}}{k_{18}}\right)-k_{21}\cdot O_3-k_{12}\cdot M\cdot O_2\cdot\frac{O}{H}-\frac{k_{32}\cdot CO}{k_{17}\cdot H}\cdot(k_{20}\cdot M\cdot O_2\cdot(1+\frac{(k_{14}-k_{15}-k_{16})\cdot H}{k_{18}\cdot O})+k_{21}\cdot O_3)). \quad (27)$$

As the result, the corrected criterion for OH equilibrium validity is as follows:

$${Crit_{OH}}^m = \frac{1}{k_{17}\cdot O}\cdot\left(\left(2\cdot k_{20}\cdot M\cdot O_2\cdot\left(1-\frac{k_{15}+k_{16}}{k_{18}}\right)+k_{21}\cdot O_3+k_{12}\cdot M\cdot O_2\cdot\frac{O}{H}+\frac{k_{32}\cdot CO}{k_{17}\cdot H}\cdot(k_{20}\cdot M\cdot O_2\cdot(1+k14-k15-k16\cdot Hk18\cdot O)+k21\cdot O3))\cdot HO\cdot k20\cdot M\cdot O2\cdot 1+2\cdot k14-k15-k16\cdot Hk18\cdot O+k21\cdot O3+k21\cdot k12\cdot M\cdot O2\cdot O-k21\cdot H\cdot O3/(k20\cdot M\cdot O_2\cdot(1+\frac{(k_{14}-k_{15}-k_{16})\cdot H}{k_{18}\cdot O})+k_{21}\cdot O_3)\leq 0.1. \quad (28)$$

We calculated this criterion using the global 3D chemical transport model and included the zonally and monthly averaged lines $<{Crit_{OH}}^m>= 0.1$ on the OH equilibrium maps (see Figure 11). One can see that including additional term actually eliminates the noted discrepancy between OH boundary and criterion. But, the application of this criterion requires CO data.

https://doi.org/10.5194/egusphere-2024-614
Preprint. Discussion started: 5 March 2024

As noted in Introduction, the conditions of nighttime OH and HO_2 equilibriums together with one for O_3 equilibrium and their analytical criteria constitute the useful tool for to retrieval these components or other characteristics (for example, O and H) from measured data. At the altitudes of upper mesosphere – lower thermosphere, these conditions can be applied, for example, to MLS/Aura database (measured characteristics: OH, HO_2, O_3, and CO), SMILES (HO_2 and O_3), SCIAMACHY ($O(^1S)$ green-line, O_2 A-band, and OH Meinel band emissions), SABER/TIMED (O_3, OH Meinel band emissions at 2.0 μm (9→7 and 8→6 bands) and at 1.6 μm (5→3 and 4→2 bands)) and other, including to improve existing retrieval approaches. In particular, Panka et al. (2021) proposed the method of simultaneous derivation of O and OH at the levels v=0-9 from SABER data (volume emission rates at 2.0 and 1.6 μm) at 80-100 km, taking into account the equilibrium condition for all states of OH. Such approach is valid for exited states due to its very low lifetimes determined by radiative transitions and quenching with O_2, N_2, and O. In the case of the OH ground state, its lifetimes determined the reaction $OH+O \rightarrow H+O_2$ only. It means that Panka et al. (2021) used an equilibrium condition for total OH, which may be significantly disrupted above 80 km in certain latitude ranges and seasons, as one can see from Figure 8. In order to check this assumption, we processed the Panka et al. (2021) data (O, OH(v=9), O_2, N_2, and temperature profiles at 80-100 km) for 2009 and calculated local profiles of $Crit_{OH}$ according to criterion (24). One can see this criterion depends of O, H, and O_3. Thus, the O_3 data was taken from SABER data collocated (via the orbit number) with the Panka et al. profiles in time and space. The H data was derived with the use of the equilibrium equation for OH(v=9):

$$a_7 \cdot O_3 \cdot H = OH(9) \cdot (a_1 + a_2 \cdot N_2 + a_3 \cdot O_2 + (a_4 + a_5 + a_6) \cdot O), \quad (29)$$

where a_{1-7} are the constant rates of processes OH(9) → OH(v≤8) + hν, OH(9) +N_2 → OH(8) + N_2, OH(9) +O_2 → OH(v≤8) + O_2, OH(9) +$O(^3P)$ → OH(v≤4) + $O(^1D)$, OH(9) +$O(^3P)$ → OH(v≤8) + $O(^3P)$, OH(v) +$O(^3P)$ → H + O_2, and H + O_3 → O_2 + OH(9), respectively. The values of a_{2-7} correspond to the Panka et al. (2021) model (see Table 1 there), the Einstein coefficients for OH(v=9) were taken from Brooke et al. (2016). Due to the strong air-concentration dependence $Crit_{OH}$ decreases rapidly with the height. From each $Crit_{OH}$ profile, we determined the local height position of the OH equilibrium boundary ($z_{OH_{sh}^{eq}}$) according to the condition $Crit_{OH} = 0.1$. It was revealed that $Crit_{OH} < 0.1$ throughout the entire altitude range for most profiles. The Figure 12 plots the found values of $z_{OH_{sh}^{eq}}$ above 80 km in different months. One can see that, in accordance of the Panka et al. data, the local height position of the OH equilibrium boundary can rise up to 87 km. Moreover, the Panka et al. method requires external data about HO_2 since the reaction $HO_2+O \rightarrow OH+O_2$ become the important source for OH below 87 km (Panka et al., 2021; see also Figure 5 in our paper). Note that the HO_2 equilibrium condition (8) depends on H and O only and can be used within the general retrieval procedure of O, H, OH(v=0-9), and HO_2,

https://doi.org/10.5194/egusphere-2024-614
Preprint. Discussion started: 5 March 2024

taking into account the criteria (16) and (24). Detailed development of this retrieval method is outside of this paper and should be carried out in a separate extended work.

8 Conclusions

The presented analysis shows that there are extended areas in mesosphere and lower thermosphere, where nighttime HO_2 and OH are close to their local equilibrium concentrations determined mainly by the reaction between HO_x – O_x components themselves and with H_2O_2, N, NO, NO_2, and CO. In upper mesosphere – lower thermosphere, the shortened expressions for their local equilibrium concentrations are valid, including the HO_x – O_x chemistry only. These conditions describes the HO_2 and OH equilibrium from the top to the some lower borders, the altitude position of which vary in the interval between 73 and 85 km and depends essentially on the season and latitude. We proposed analytical criteria, which almost everywhere well reproduces the main features of these borders. The obtained results allow extending the abilities of the Panka et al. (2021) method of retrieval of unmeasured components from SABER data. The simultaneous application of OH and HO_2 equilibrium conditions to the SABER data (O_3, volume emission rates at 2.0 and 1.6 μm) together with the criteria (16) and (24) to control this equilibrium validity is going to retrieve all unknown HO_x – O_x components (O, H, OH, and HO_2), extending the altitude range of retrieval below 80 km and without external information.

Data availability. The Panka et al. data are obtained from the SABER website (https://saber.gats-inc.com).

Code availability. Code is available upon request.

Author contributions. MK and MB carried out the data processing and analysis and wrote the manuscript. AC, SD, and AM contributed to reviewing the article.

Competing interests. The authors declare that they have no conflict of interest.

Acknowledgements.

https://doi.org/10.5194/egusphere-2024-614
Preprint. Discussion started: 5 March 2024

Financial support. This work was supported by the Russian Science Foundation under grant No. 22-12-00064 (https://rscf.ru/project/22-12-00064/) and state assignment no. 0729-2020-0037.

References

Belikovich, M. V., Kulikov, M. Yu, Grygalashvyly, M., Sonnemann, G. R., Ermakova, T. S., Nechaev, A. A., and Feigin, A .M.: Ozone chemical equilibrium in the extended mesopause under the nighttime conditions, Adv. Space Res., 61, 426–432, https://doi.org/10.1016/j.asr.2017.10.010, 2018.

Berger, U., and U. von Zahn (1999), Two level structure of the mesopause: A model study, *J. Geophys. Res.*, 104, 22,083–22,093.

Brooke, J. S., Bernath, P. F., Western, C. M., Sneden, C., Afşar, M., Li, G., and Gordon, I. E.: Line strengths of rovibrational and rotational transitions in the $X^2\Pi$ ground state of OH, Journal of Quantitative Spectroscopy and Radiative Transfer, 168, 142–157, https://doi.org/10.1016/j.jqsrt.2015.07.021, 2016.

Burkholder, J. B., Sander, S. P., Abbatt, J., Barker, J. R., Cappa, C., Crounse, J. D., Dibble, T. S., Huie, R. E., Kolb, C. E., Kurylo, M. J., Orkin, V. L., Percival, C. J., Wilmouth, D. M., and Wine, P. H.: Chemical Kinetics and Photochemical Data for Use in Atmospheric Studies, Evaluation No. 19, JPL Publication 19-5, Jet Propulsion Laboratory, Pasadena, http://jpldataeval.jpl.nasa.gov, 2020.

Evans, W. F. J., and Llewellyn, E. J.: Atomic hydrogen concentrations in the mesosphere and the hydroxyl emissions, J. Geophys. Res., 78, 323–326, https://doi.org/1010.1029/JA078i001p00323, 1973.

Evans, W. F. J., McDade, I. C., Yuen, J., and Llewellyn, E. J.: A rocket measurement of the O_2 infrared atmospheric (0-0) band emission in the dayglow and a determination of the mesospheric ozone and atomic oxygen densities, Can. J. Phys., 66, 941–946, https://doi.org/10.1139/p88-151. 1988.

Fytterer, T., von Savigny, C., Mlynczak, M., and Sinnhuber, M.: Model results of OH airglow considering four different wavelength regions to derive night-time atomic oxygen and atomic hydrogen in the mesopause region, Atmos. Chem. Phys., 19, 1835–1851, https://doi.org/10.5194/acp-19-1835-2019, 2019.

Good, R. E.: Determination of atomic oxygen density from rocket borne measurements of hydroxyl airglow, Planet. Space Sci., 24, 389–395, https://doi.org/10.1016/0032-0633(76)90052-0, 1976.

Grygalashvyly, M., Sonnemann, G. R., and Hartogh, P.: Long-term behavior of the concentration of the minor constituents in the mesosphere - A model study, Atmos. Chem. Phys., 9, 2779–2792, https://doi.org/10.5194/acp-9-2779-2009, 2009.

Grygalashvyly, M., Sonnemann, G. R., Lübken, F.-J., Hartogh, P., and Berger, U.: Hydroxyl layer: Mean state and trends at midlatitudes, J. Geophys. Res. Atmos., 119, 12,391–12,419, https://doi.org/10.1002/2014JD022094, 2014.

https://doi.org/10.5194/egusphere-2024-614
Preprint. Discussion started: 5 March 2024

Grygalashvyly, M.: Several notes on the OH* layer, Ann. Geophys., 33, 923-930, https://doi.org/10.5194/angeo-33-923-2015, 2015.

Hartogh, P., Jarchow, C., Sonnemann, G. R., and Grygalashvyly, M.: On the spatiotemporal behavior of ozone within the upper mesosphere/mesopause region under nearly polar night conditions, J. Geophys. Res., 109, D18303, https://doi.org/10.1029/2004JD004576, 2004.

Hartogh, P., Jarchow, Ch., Sonnemann, G. R., and Grygalashvyly, M.: Ozone distribution in the middle latitude mesosphere as derived from microwave measurements at Lindau (51.66°N, 10.13°E), J. Geophys. Res., 116, D04305, https://doi.org/10.1029/2010JD014393, 2011.

Körner, U., and Sonnemann, G. R.: Global 3D-modeling of water vapor concentration of the mesosphere/mesopause region and implications with respect to the NLC region, J. Geophys. Res., 106, 9639– 9651, https://doi.org/10.1029/2000JD900744, 2001.

Kowalewski, S., v. Savigny, C., Palm, M., McDade, I. C., and Notholt, J.: On the impact of the temporal variability of the collisional quenching process on the mesospheric OH emission layer: a study based on SD-WACCM4 and SABER, Atmos. Chem. Phys., 14, 10193-10210, https://doi.org/10.5194/acp-14-10193-2014, 2014.

Kremp, C., Berger, U., Hoffmann, P., Keuer, D., and Sonnemann, G. R.: Seasonal variation of middle latitude wind fields of the mesopause region—A comparison between observation and model calculation, Geophys. Res. Lett., 26, 1279–1282, https://doi.org/10.1029/1999GL900218, 1999.

Kulikov, M. Y., Feigin, A. M., and Sonnemann, G. R.: Retrieval of the vertical distribution of chemical components in the mesosphere from simultaneous measurements of ozone and hydroxyl distributions, Radiophys. Quantum Electron., 49, 683–691, https://doi.org/10.1007/s11141-006-0103-4, 2006.

Kulikov, M. Yu., Feigin, A. M., and Sonnemann, G. R.: Retrieval of water vapor profile in the mesosphere from satellite ozone and hydroxyl measurements by the basic dynamic model of mesospheric photochemical system, Atmos. Chem. Phys., 9, 8199–8210, https://doi.org/10.5194/acp-9-8199-2009, 2009.

Kulikov, M. Y., Belikovich, M. V., Grygalashvyly, M., Sonnemann, G. R., Ermakova, T. S., Nechaev, A. A., and Feigin, A. M.: Daytime ozone loss term in the mesopause region, Ann. Geophys., 35, 677-682 https://doi.org/10.5194/angeo-35-677-2017, 2017.

Kulikov, M. Y., Nechaev, A. A., Belikovich, M. V., Ermakova, T. S., and Feigin, A. M.: Technical note: Evaluation of the simultaneous measurements of mesospheric OH, HO_2, and O_3 under a photochemical equilibrium assumption – a statistical approach, Atm. Chem. Phys., 18, 7453-747, https://doi.org/10.5194/acp-18-7453-2018, 2018a.

Kulikov, M. Y., Belikovich, M. V., Grygalashvyly, M., Sonnemann, G. R., Ermakova, T. S., Nechaev, A. A., and Feigin, A. M.: Nighttime ozone chemical equilibrium in the mesopause region. J. Geophys. Res.,123, 3228–3242, https://doi.org/10.1002/2017JD026717, 2018b.

https://doi.org/10.5194/egusphere-2024-614
Preprint. Discussion started: 5 March 2024

Kulikov, M. Yu., Nechaev, A. A., Belikovich, M. V., Vorobeva, E. V., Grygalashvyly, M., Sonnemann, G. R., and Feigin, A. M.: Border of nighttime ozone chemical equilibrium in the mesopause region from saber data: implications for derivation of atomic oxygen and atomic hydrogen, Geophys. Res. Lett., 46, 997– 1004, https://doi.org/10.1029/2018GL080364, 2019.

Kulikov, M. Y., Belikovich, M. V., Feigin, A. M.: The 2-day photochemical oscillations in the mesopause region: the first experimental evidence? Geophys. Res. Lett., 48, e2021GL092795, https://doi.org/10.1029/2021GL092795, 2021.

Kulikov M.Yu., Belikovich, M.V., Grygalashvyly, M., Sonnemann, G. R., and Feigin, A.M.: Retrieving daytime distributions of O, H, OH, HO_2, and chemical heating rate in the mesopause region from satellite observations of ozone and OH* volume emission: The evaluation of the importance of the reaction $H+O_3 \rightarrow O_2+OH$ in the ozone balance, Adv. Space Res., 69(9), 3362-3373, https://doi.org/10.1016/j.asr.2022.02.011, 2022a.

Kulikov, M. Y., Belikovich, M. V., Grygalashvyly, M., Sonnemann, G. R., and Feigin, A.M.: The revised method for retrieving daytime distributions of atomic oxygen and odd-hydrogens in the mesopause region from satellite observations, Earth, Planets and Space, 74, 44, https://doi.org/10.1186/s40623-022-01603-8, 2022b.

Kulikov, M. Yu., Belikovich, M. V., Chubarov, A. G., Dementeyva, S. O., Feigin, A. M.: Boundary of nighttime ozone chemical equilibrium in the mesopause region: improved criterion of determining the boundary from satellite data, Adv. Space Res., 71 (6), 2770-2780, https://doi.org/10.1016/j.asr.2022.11.005, 2023a.

Kulikov, M. Yu., Belikovich, M. V., Chubarov, A. G., Dementyeva, S. O., and Feigin, A. M.: Boundary of nighttime ozone chemical equilibrium in the mesopause region: long-term evolution determined using 20-year satellite observations, Atmos. Chem. Phys., 23, 14593–14608, https://doi.org/10.5194/acp-23-14593-2023, 2023b.

Llewellyn, E. J., McDade, I. C. Moorhouse, P. and Lockerbie M. D.: Possible reference models for atomic oxygen in the terrestrial atmosphere, Adv. Space Res., 13, 135–144, https://doi.org/10.1016/0273-1177(93)90013-2, 1993.

Llewellyn, E. J., and McDade, I. C.: A reference model for atomic oxygen in the terrestrial atmosphere, Adv. Space Res., 18, 209–226, https://doi.org/10.1016/0273-1177(96)00059-2, 1996.

Manney, G. L., Kruger, K., Sabutis, J. L., Sena, S. A., and Pawson, S.: The remarkable 2003–2004 winter and other recent warm winters in the Arctic stratosphere since the late 1990s. J. Geophys. Res., 110, D04107, https://doi.org/10.1029/2004JD005367, 2005.

Marsh, D. R., Smith, A. K., Mlynczak, M. G., and Russell III, J. M.: SABER observations of the OH Meinel airglow variability near the mesopause, J. Geophys. Res., 111, A10S05, https://doi.org/10.1029/2005JA011451, 2006.

https://doi.org/10.5194/egusphere-2024-614
Preprint. Discussion started: 5 March 2024

McDade, I. C., Llewellyn, E. J., and Harris, F. R.: Atomic oxygen concentrations in the lower auroral thermosphere, Adv. Space Res., 5, 229–232, https://doi.org/10.1029/GL011I003P00247, 1985.

McDade, I. C., and Llewellyn, E. J.: Mesospheric oxygen atom densities inferred from night-time OH Meinel band emission rates, Planet. Space Sci., 36, 897–905, https://doi.org/10.1016/0032-0633(88)90097-9, 1988.

Mlynczak, M. G., Marshall, B. T., Martin-Torres, F. J., Russell III, J. M., Thompson, R. E., Remsberg, E. E., and Gordley, L. L.: Sounding of the Atmosphere using Broadband Emission Radiometry observations of daytime mesospheric $O_2(^1D)$ 1.27 μm emission and derivation of ozone, atomic oxygen, and solar and chemical energy deposition rates, J. Geophys. Res., 112, D15306, https://doi.org/10.1029/2006JD008355, 2007.

Mlynczak, M. G., Hunt, L. A., Mast, J. C., Marshall, B. T., Russell III, J. M., Smith, A. K., Siskind, D. E., Yee, J.-H., Mertens, C. J., Martin-Torres, F. J., Thompson, R. E., Drob, D. P., and Gordley, L. L.: Atomic oxygen in the mesosphere and lower thermosphere derived from SABER: Algorithm theoretical basis and measurement uncertainty, J. Geophys. Res., 118, 5724–5735, https://doi.org/10.1002/jgrd.50401, 2013a.

Mlynczak, M. G., Hunt, L. H., Mertens, C. J., Marshall, B. T., Russell III, J. M., López-Puertas, M., Smith, A. K., Siskind, D. E., Mast, J. C., Thompson, R. E., and Gordley, L. L.: Radiative and energetic constraints on the global annual mean atomic oxygen concentration in the mesopause region, J. Geophys. Res. Atmos., 118, 5796–5802, https://doi.org/10.1002/jgrd.50400, 2013b.

Mlynczak, M. G., Hunt, L. A. Marshall, B. T. Mertens, C. J. Marsh, D. R. Smith, A. K. Russell, J. M. Siskind D. E., and Gordley L. L.: Atomic hydrogen in the mesopause region derived from SABER: Algorithm theoretical basis, measurement uncertainty, and results, J. Geophys. Res., 119, 3516–3526, https://doi.org/10.1002/2013JD021263, 2014.

Mlynczak, M. G., Hunt, L. A., Russell, J. M. III, and Marshall, B. T.: Updated SABER night atomic oxygen and implications for SABER ozone and atomic hydrogen, Geophys. Res. Lett., 45, 5735–5741, https://doi.org/10.1029/2018GL077377, 2018.

Morton, K. W., and Mayers, D. F.; Numerical Solution of Partial Differential Equations, Cambridge University Press, 1994.

Nikoukar, R., Swenson, G. R., Liu, A. Z., and Kamalabadi, F.: On the variability of mesospheric OH emission profiles, J. Geophys. Res., 112, D19109, https://doi.org/10.1029/2007JD008601, 2007.

Panka, P. A., Kutepov, A. A., Zhu, Y., Kaufmann, M., Kalogerakis, K. S., Rezac, L., et al.: Simultaneous retrievals of nighttime $O(^3P)$ and total OH densities from satellite observations of Meinel band emissions. Geoph. Res.Lett., 48, e2020GL091053, https://doi.org/10.1029/2020GL091053, 2021.

Pendleton, W. R., Baker, K. D., Howlett, L. C.: Rocket-based investigations of $O(^3P)$, O_2 ($a^1\Delta_g$) and OH* (v=1,2) during the solar eclipse of 26 February 1979, J. Atm. Terr. Phys., 45(7), 479-491, 1983.

https://doi.org/10.5194/egusphere-2024-614
Preprint. Discussion started: 5 March 2024

Siskind, D. E., Marsh, D. R., Mlynczak, M. G., Martin-Torres, F. J., and Russell III, J. M.: Decreases in atomic hydrogen over the summer pole: Evidence for dehydration from polar mesospheric clouds? Geophys. Res. Lett., 35, L13809, https://doi.org/10.1029/2008GL033742, 2008.

Russell, J. P., and Lowe, R. P.: Atomic oxygen profiles (80-94 km) derived from Wind Imaging Interferometer/Upper Atmospheric Research Satellite measurements of the hydroxyl airglow: 1. Validation of technique, J. Geophys. Res., 108(D21), 4662, https://doi.org/10.1029/2003JD003454, 2003.

Russell, J. P., Ward, W. E., Lowe, R. P., Roble, R. G., Shepherd, G. G., and Solheim, B.: Atomic oxygen profiles (80 to 115 km) derived from Wind Imaging Interferometer/Upper Atmospheric Research Satellite measurements of the hydroxyl and green line airglow: Local time–latitude dependence, J. Geophys. Res., 110(D15), D15305, https://doi.org/10.1029/2004JD005570, 2005.

Siskind, D. E., Mlynczak, M. G., Marshall, T., Friedrich, M., Gumbel, J.: Implications of odd oxygen observations by the TIMED/SABER instrument for lower D region ionospheric modeling, J. Atmos. Sol. Terr. Phys., 124, 63–70, https://doi.org/10.1016/j.jastp.2015.01.014, 2015.

Smith, A. K., Lopez-Puertas, M., Garcıa-Comas, M. and Tukiainen, S.: SABER observations of mesospheric ozone during NH late winter 2002–2009, Geophys. Res. Lett., 36, L23804, https://doi.org/10.1029/2009GL040942, 2009.

Smith, A. K., Marsh, D. R. Mlynczak, M. G. and Mast, J. C.: Temporal variations of atomic oxygen in the upper mesosphere from SABER, J. Geophys. Res., 115, D18309, https://doi.org/10.1029/2009JD013434, 2010.

Sonnemann, G., Kremp, C. Ebel, A. and Berger U.: A three-dimensional dynamic model of minor constituents of the mesosphere, Atmos. Environ., 32, 3157–3172, https://doi.org/10.1016/S1352-2310(98)00113-7, 1998.

Sonnemann, G. R., Grygalashvyly, M., Hartogh, P., and Jarchow, C.: Behavior of mesospheric ozone under nearly polar night conditions, Adv. Space Res., 38, 2402–2407, https://doi.org/10.1016/j.asr.2006.09.011, 2006.

Sonnemann, G. R., Hartogh, P., Grygalashvyly, M., Li, S., and Berger, U.: The quasi 5-day signal in the mesospheric water vapor concentration at high latitudes in 2003-a comparison between observations at ALOMAR and calculations, J. Geophys. Res., 113, D04101, https://doi.org/10.1029/2007JD008875, 2008.

Sonnemann, G. R., Hartogh, P., Berger, U., and Grygalashvyly, M.: Hydroxyl layer: trend of number density and intra-annual variability, Ann. Geophys., 33, 749–767, https://doi.org/10.5194/angeo-33-749-2015, 2015.

Swenson, G. R., and Gardner C. S.: Analytical models for the responses of the mesospheric OH* and Na layers to atmospheric gravity waves, J. Geophys. Res., 103(D6), 6271–6294, https://doi.org/10.1029/97JD02985, 1998.

https://doi.org/10.5194/egusphere-2024-614
Preprint. Discussion started: 5 March 2024

613 Thomas, R. J.: Atomic hydrogen and atomic oxygen density in the mesosphere region: Global and
614 seasonal variations deduced from Solar Mesosphere Explorer near-infrared emissions, J. Geophys. Res.,
615 95, 16,457–16,476, https://doi. org/ 10. 1029/ JD095 iD10p 16457, 1990.
616 Walcek, C. J.: Minor flux adjustment near mixing ratio extremes for simplified yet highly accurate
617 monotonic calculation of tracer advection, J. Geophys. Res., 105, 9335-9348,
618 https://doi.org/10.1029/1999JD901142, 2000.
619 Xu, J., Smith, A. K., Jiang, G., Gao, H., Wei, Y., Mlynczak, M. G., and Russell III, J. M.: Strong
620 longitudinal variations in the OH nightglow, Geophys. Res. Lett., 37, L21801,
621 https://doi.org/10.1029/2010GL043972, 2010.
622 Xu, J., Gao, H. Smith, A. K. and Zhu Y.: Using TIMED/SABER nightglow observations to investigate
623 hydroxyl emission mechanisms in the mesopause region, J. Geophys. Res., 117, D02301,
624 https://doi.org/10.1029/2011JD016342, 2012.

https://doi.org/10.5194/egusphere-2024-614
Preprint. Discussion started: 5 March 2024

Table 1. List of reactions included in 3-d chemical transport model with the corresponding reaction rates taken from Burkholder et al. (2020).

1	$O(^1D)+O_2 \rightarrow O+O_2$	24	$H+OH+N_2 \rightarrow H_2O+N_2$	47	$NO+O_3 \rightarrow NO_2+O_2$
2	$O(^1D)+N_2 \rightarrow O+N_2$	25	$OH+H_2 \rightarrow H_2O+H$	48	$NO_2+O_3 \rightarrow NO_3+O_2$
3	$O(^1D)+O_3 \rightarrow O_2+2O$	26	$OH+OH \rightarrow H_2O+O$	49	$N+OH \rightarrow NO+H$
4	$O(^1D)+O_3 \rightarrow 2O_2$	27	$OH+OH+M \rightarrow H_2O_2+M$	50	$NO+HO_2 \rightarrow NO_2+OH$
5	$O(^1D)+N_2O \rightarrow 2NO$	28	$OH+HO_2 \rightarrow H_2O+O_2$	51	$H+NO_2 \rightarrow OH+NO$
6	$O(^1D)+N_2O \rightarrow N_2+O_2$	29	$H_2O_2+OH \rightarrow H_2O+HO_2$	52	$NO_3+NO \rightarrow 2NO_2$
7	$O(^1D)+H_2O \rightarrow 2OH$	30	$HO_2+HO_2 \rightarrow H_2O_2+O_2$	53	$N+NO \rightarrow N_2+O$
8	$O(^1D)+H_2 \rightarrow H+OH$	31	$HO_2+HO_2+M \rightarrow H_2O_2+O_2+M$	54	$N+NO_2 \rightarrow N_2O+O$
9	$O(^1D)+CH_4 \rightarrow CH_3+OH$	32	$OH+CO \rightarrow H+CO_2$	55	$O_2+h\nu \rightarrow 2O$
10	$O(^1D)+CH_4 \rightarrow H_2+CH_2O$	33	$CH_4+OH \rightarrow CH_3+H_2O$	56	$O_2+h\nu \rightarrow O+O(^1D)$
11	$O+O+M \rightarrow O_2+M$	34	$CH_3+O_2 \rightarrow CH_3O_2$	57	$O_3+h\nu \rightarrow O_2+O$
12	$O+O_2+M \rightarrow O_3+M$	35	$CH_3+O \rightarrow CH_2O+H$	58	$O_3+h\nu \rightarrow O_2+O(^1D)$
13	$O+O_3 \rightarrow O_2+O_2$	36	$CH_3O_2+NO \rightarrow CH_3O+NO_2$	59	$N_2+h\nu \rightarrow 2N$
14	$H+HO_2 \rightarrow 2OH$	37	$CH_3O+O_2 \rightarrow CH_2O+HO_2$	60	$NO+h\nu \rightarrow N+O$
15	$H+HO_2 \rightarrow H_2O+O$	38	$CH_2O \rightarrow H_2+CO$	61	$NO_2+h\nu \rightarrow NO+O$
16	$H+HO_2 \rightarrow H_2+O_2$	39	$CH_2O \rightarrow H+CHO$	62	$N_2O+h\nu \rightarrow N_2+O(^1D)$
17	$OH+O \rightarrow H+O_2$	40	$CHO+O_2 \rightarrow HO_2+CO$	63	$N_2O+h\nu \rightarrow N+NO$
18	$HO_2+O \rightarrow OH+O_2$	41	$O_3+N \rightarrow NO+O_2$	64	$NO_3+h\nu \rightarrow NO_2+O$
19	$H_2O_2+O \rightarrow OH+HO_2$	42	$NO_3+O \rightarrow NO_2+O_2$	65	$H_2O+h\nu \rightarrow H+OH$
20	$H+O_2+M \rightarrow HO_2+M$	43	$O+NO+M \rightarrow NO_2+M$	66	$H_2O_2+h\nu \rightarrow 2OH$
21	$H+O_3 \rightarrow OH+O_2$	44	$NO_2+O \rightarrow NO+O_2$	67	$CH_4+h\nu \rightarrow CH_2+H_2$
22	$OH+O_3 \rightarrow O_2+HO_2$	45	$NO_2+O+M \rightarrow NO_3+M$	68	$CH_4+h\nu \rightarrow CH+H_2+H$
23	$HO_2+O_3 \rightarrow OH+2O_2$	46	$N+O_2 \rightarrow NO+O$	69	$CO_2+h\nu \rightarrow CO+O$

https://doi.org/10.5194/egusphere-2024-614
Preprint. Discussion started: 5 March 2024

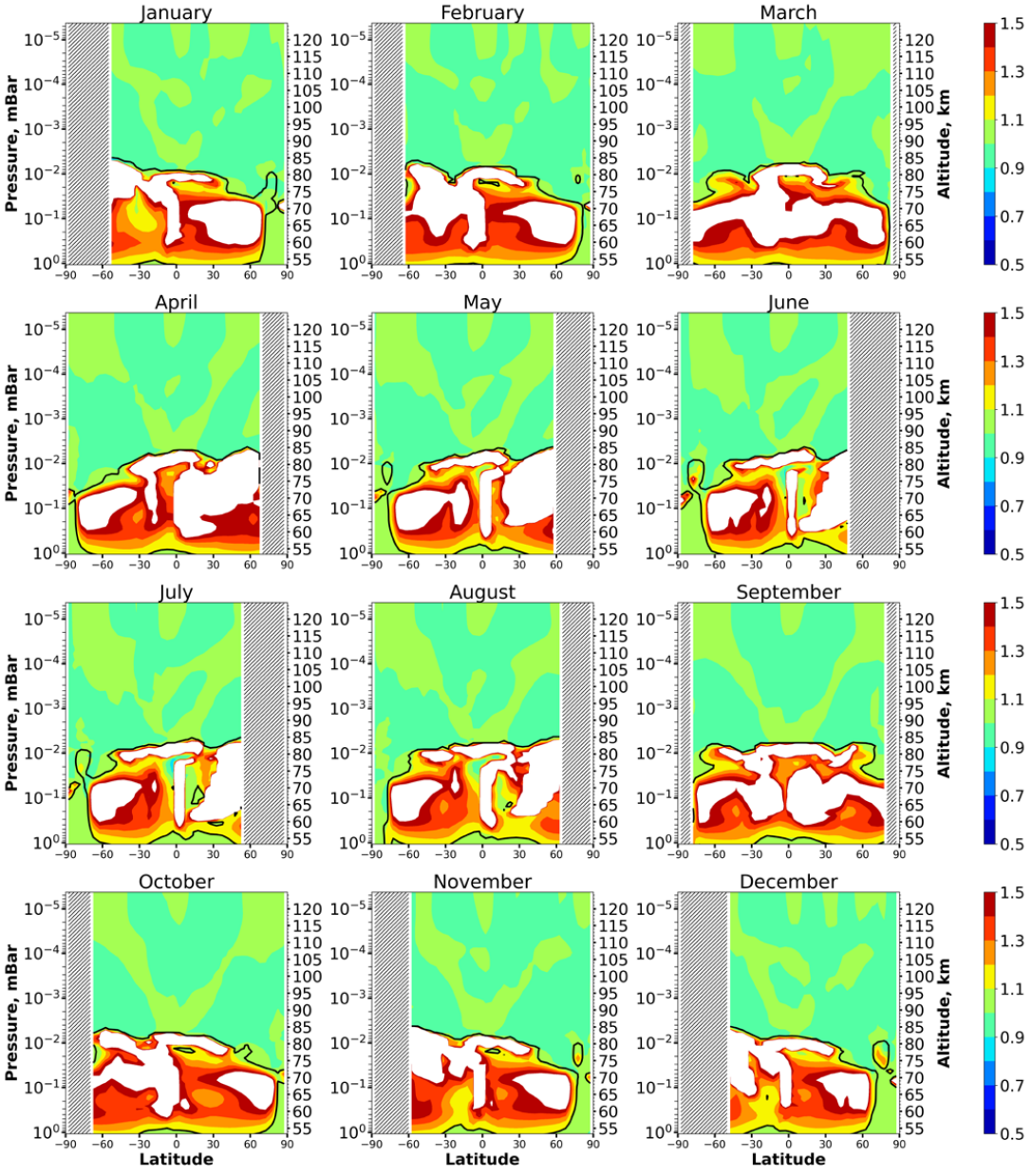

629

630 Figure 1. Nighttime mean and monthly averaged $HO_2/HO_2{}^{eq}$. Black line shows the border of HO_2

631 equilibrium according to condition (1).

632

https://doi.org/10.5194/egusphere-2024-614
Preprint. Discussion started: 5 March 2024

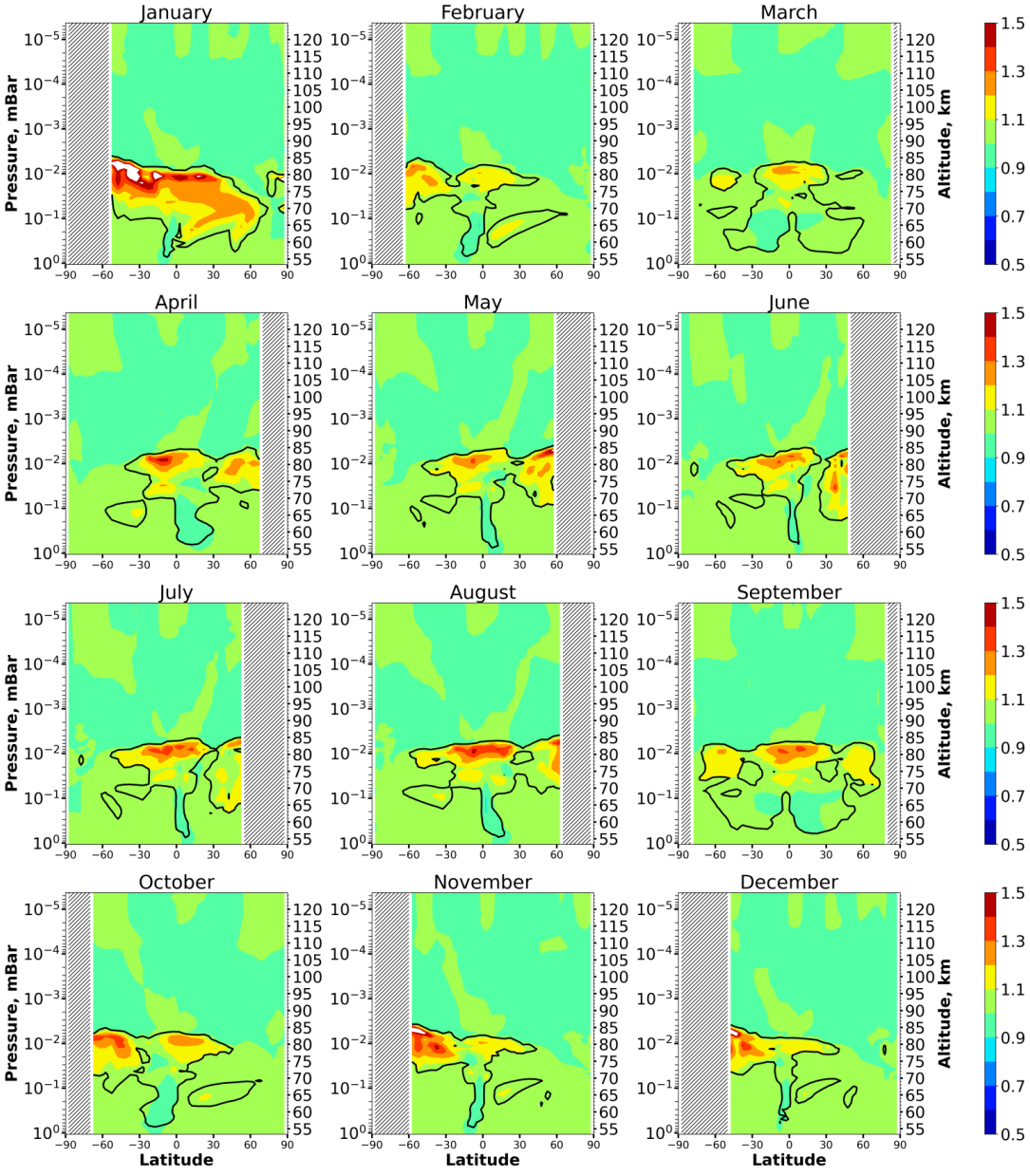

633

634 Figure 2. Nighttime mean and monthly averaged OH/OH^{eq}. Black line shows the border of OH

635 equilibrium according to condition (1).

636

https://doi.org/10.5194/egusphere-2024-614
Preprint. Discussion started: 5 March 2024

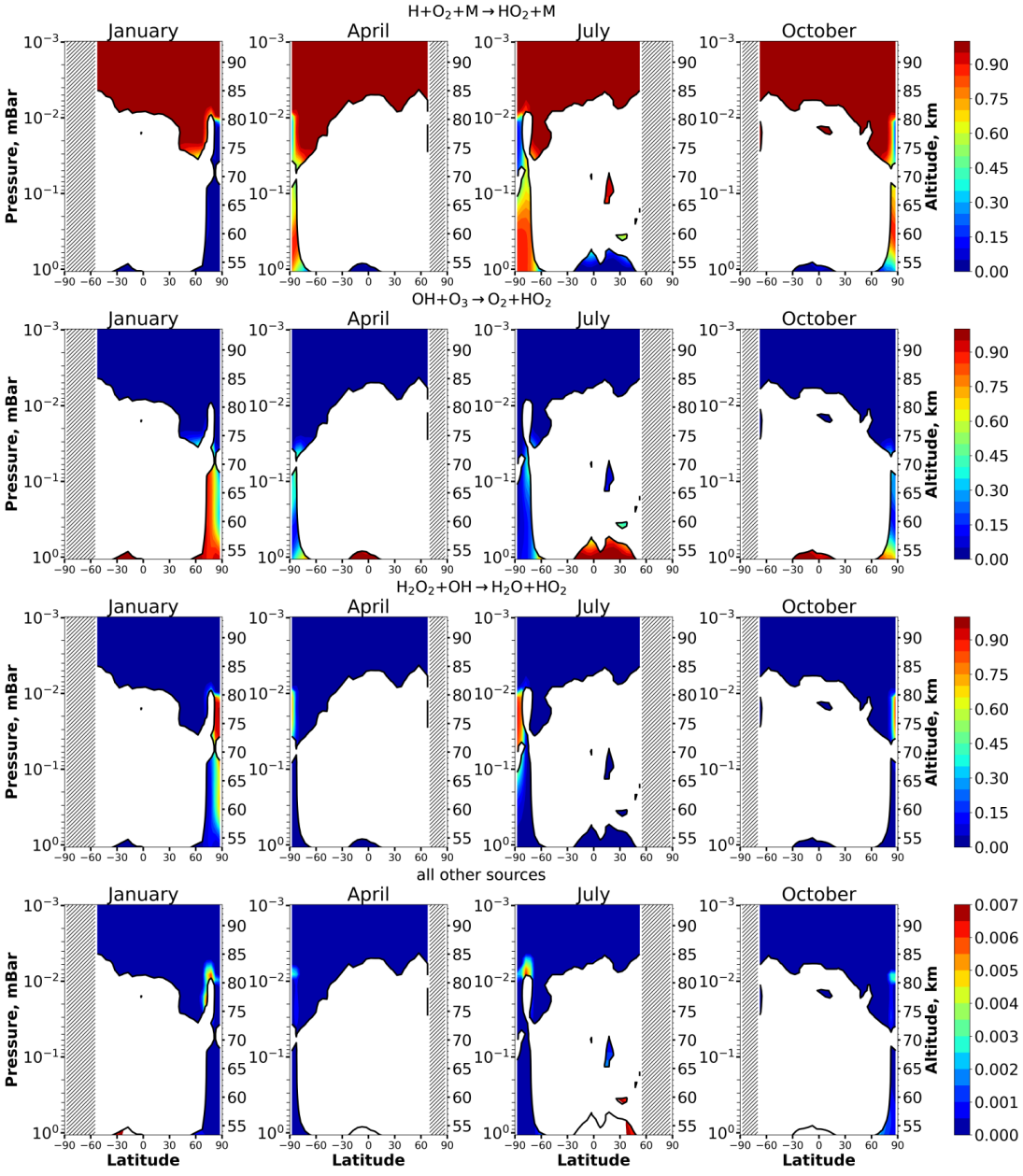

637

638 Figure 3. Nighttime mean and monthly averaged the relative contribution of a certain reaction to the total
639 source of HO_2 in equilibrium areas. White color points nonequilibrium areas of HO_2.

640

https://doi.org/10.5194/egusphere-2024-614
Preprint. Discussion started: 5 March 2024

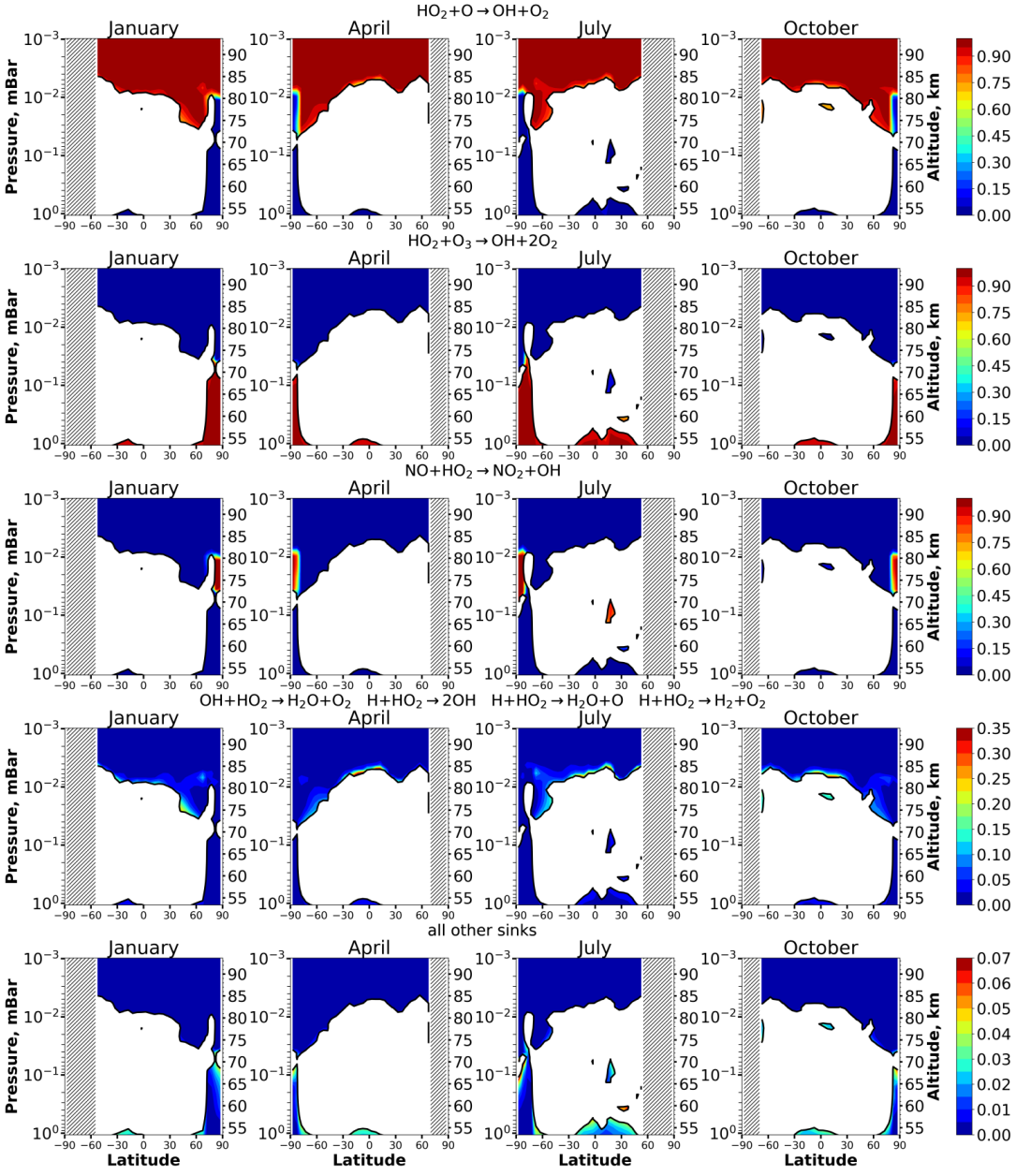

641

642 Figure 4. Nighttime mean and monthly averaged the relative contribution of a certain reaction to the total
643 sink of HO_2 in equilibrium areas. White color points nonequilibrium areas of HO_2.

644

https://doi.org/10.5194/egusphere-2024-614
Preprint. Discussion started: 5 March 2024

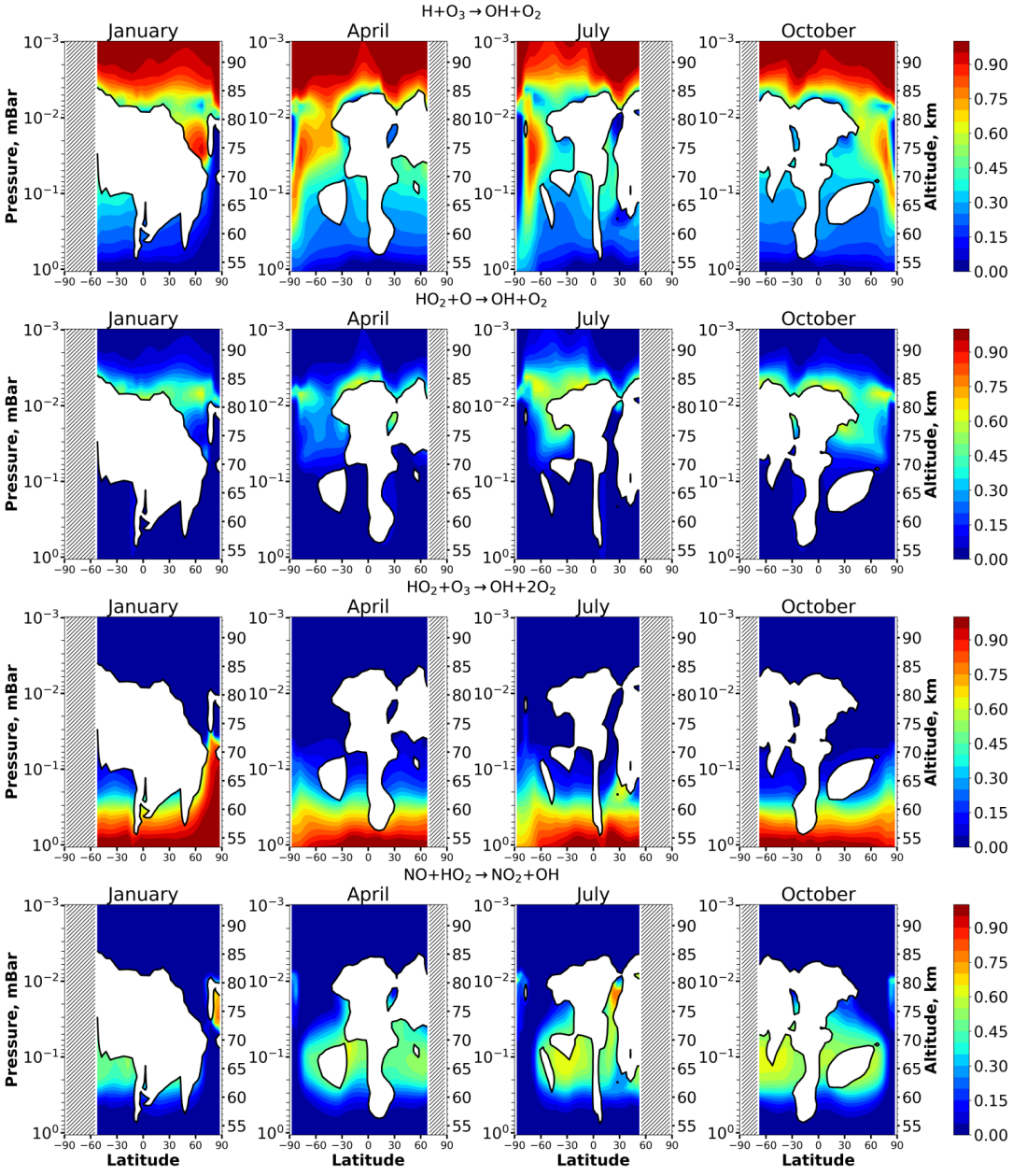

Figure 5. Nighttime mean and monthly averaged the relative contribution of a certain reaction to the total source of OH in equilibrium areas (first part). White color points nonequilibrium areas of OH.

https://doi.org/10.5194/egusphere-2024-614
Preprint. Discussion started: 5 March 2024

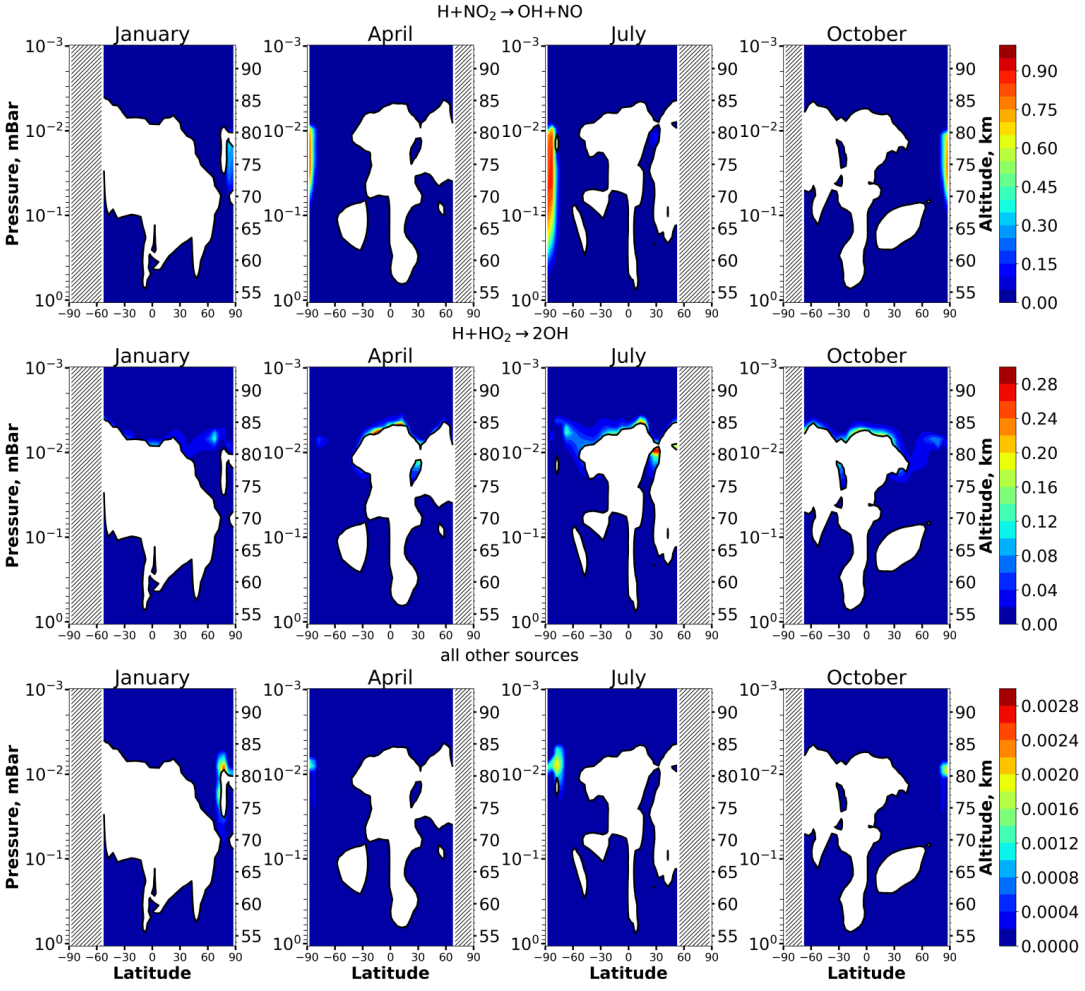

Figure 6. Nighttime mean and monthly averaged the relative contribution of a certain reaction to the total source of OH in equilibrium areas (second part). White color points nonequilibrium areas of OH.

https://doi.org/10.5194/egusphere-2024-614
Preprint. Discussion started: 5 March 2024

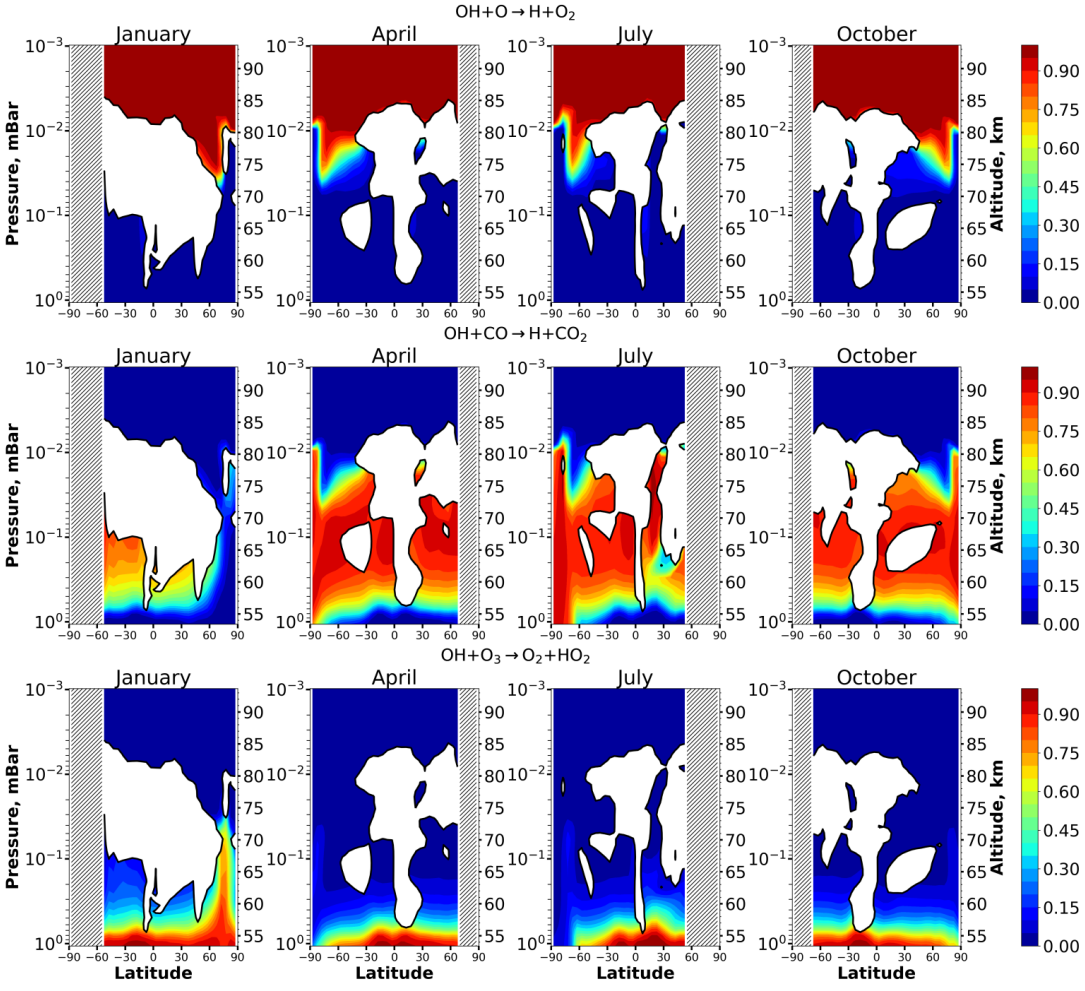

Figure 7. Nighttime mean and monthly averaged the relative contribution of a certain reaction to the total sink of OH in equilibrium areas (first part). White color points nonequilibrium areas of OH.

https://doi.org/10.5194/egusphere-2024-614
Preprint. Discussion started: 5 March 2024

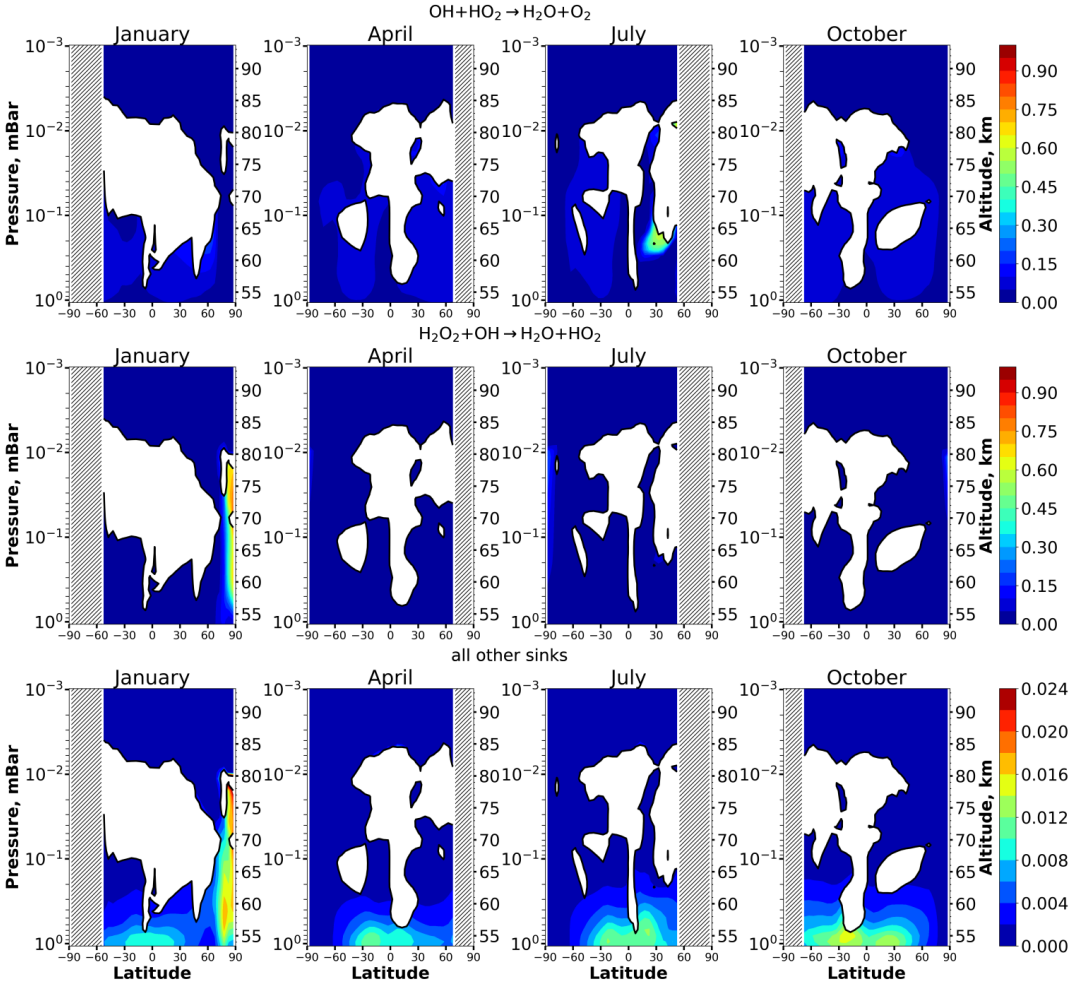

Figure 8. Nighttime mean and monthly averaged the relative contribution of a certain reaction to the total source of OH in equilibrium areas (second part). White color points nonequilibrium areas of OH.

https://doi.org/10.5194/egusphere-2024-614
Preprint. Discussion started: 5 March 2024

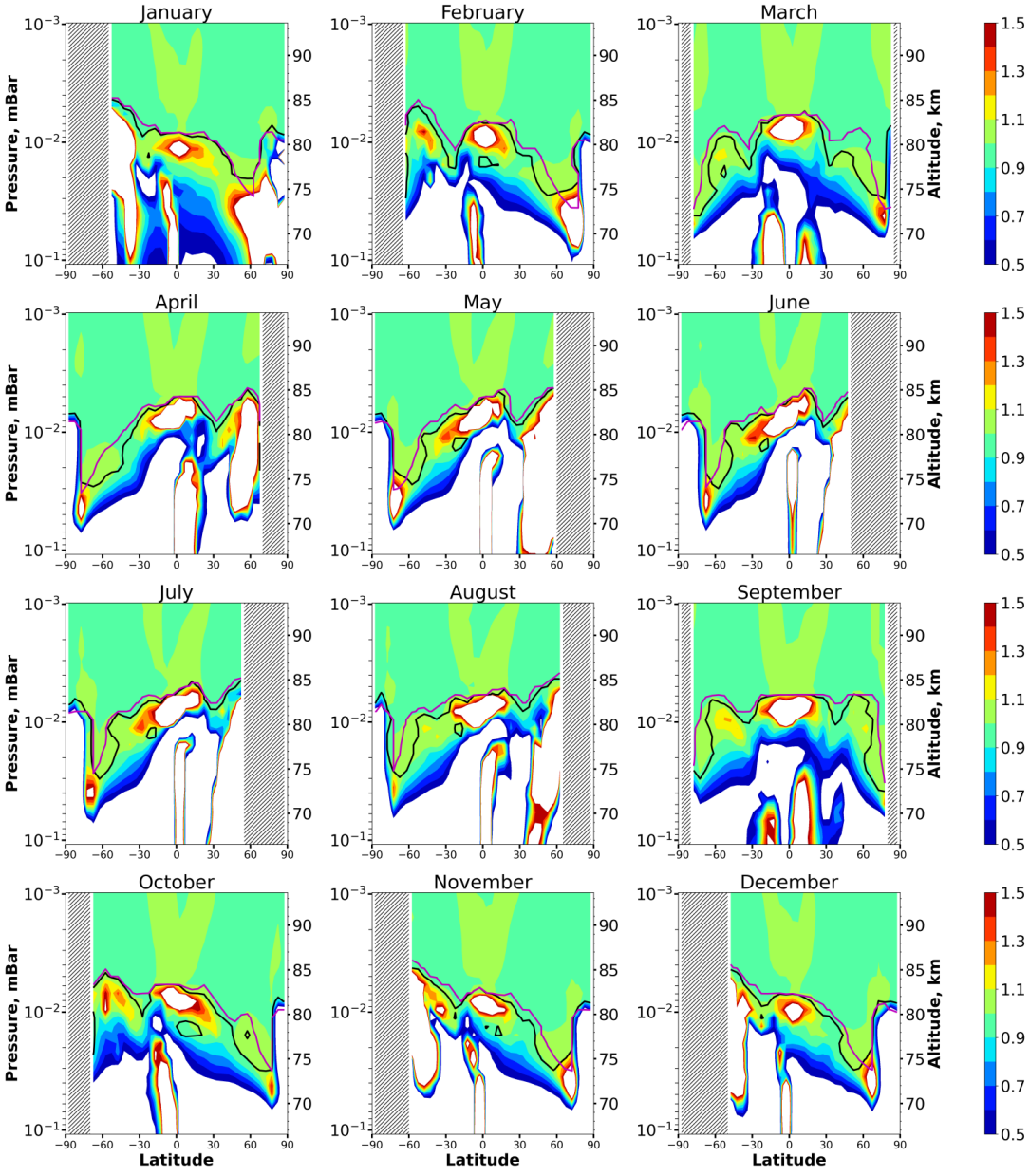

Figure 9. Nighttime mean and monthly averaged $HO_2/HO_{2_{sh}}^{eq}$. Black line shows the border of HO_2 equilibrium according to condition (1). Magenta line shows $< Crit_{HO_2} >= 0.1$.

https://doi.org/10.5194/egusphere-2024-614
Preprint. Discussion started: 5 March 2024

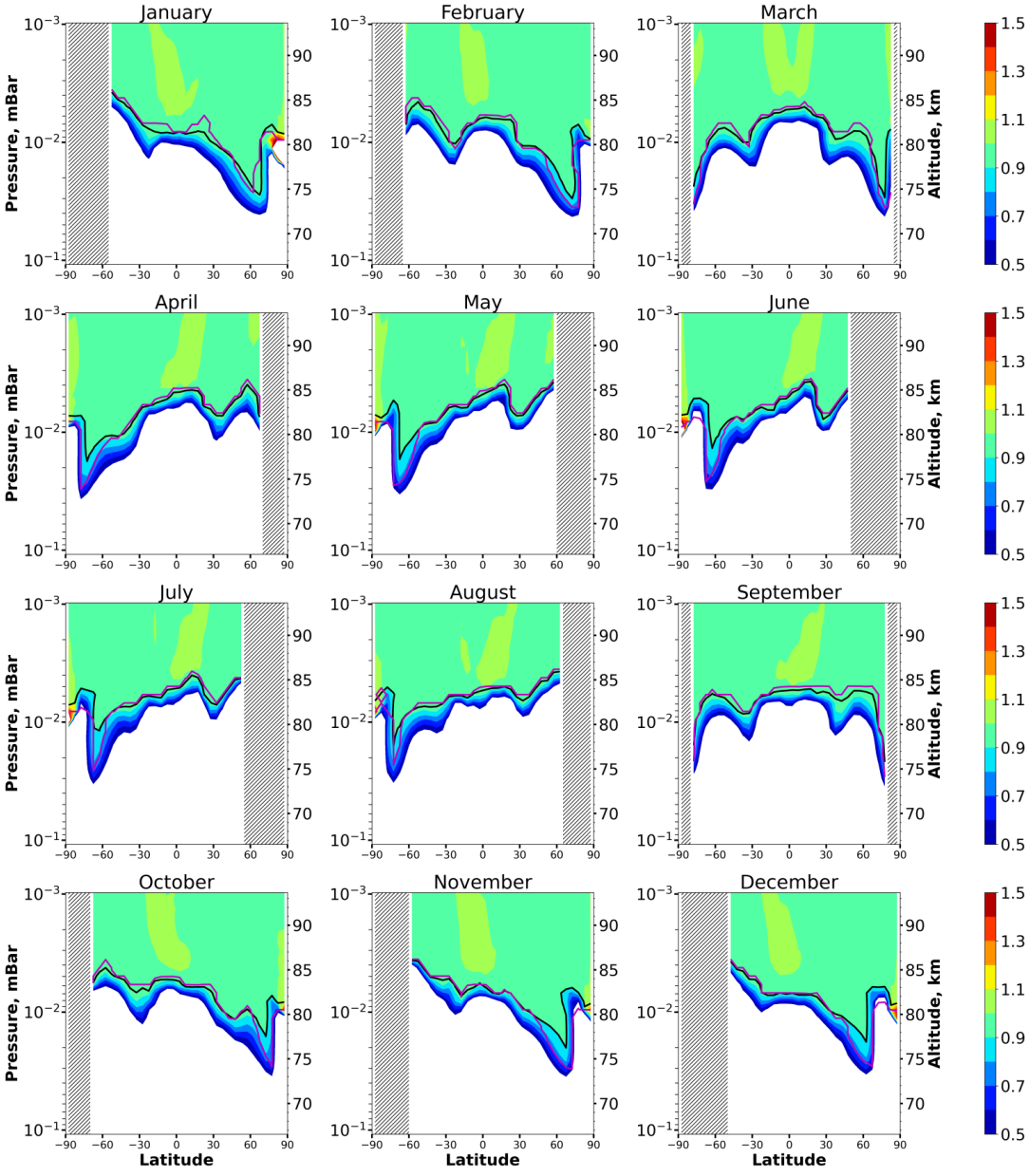

Figure 10. Nighttime mean and monthly averaged OH/OH_{sh}^{eq}. Black line shows the border of OH equilibrium according to condition (1). Magenta line shows $< Crit_{OH} >= 0.1$.

https://doi.org/10.5194/egusphere-2024-614
Preprint. Discussion started: 5 March 2024

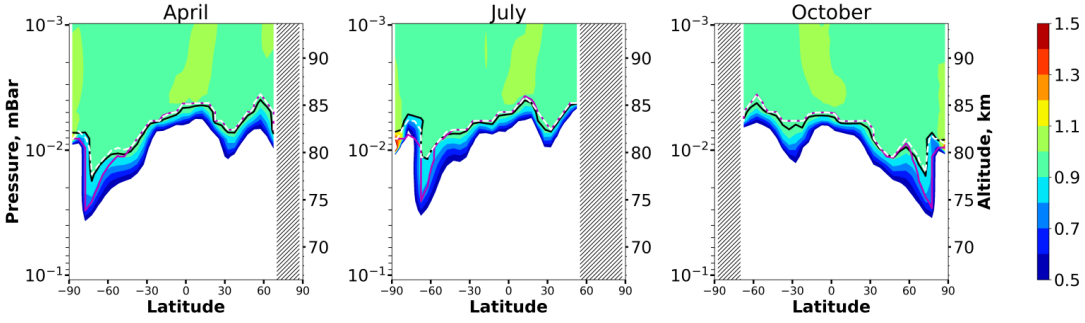

671

672 Figure 11. Nighttime mean and monthly averaged OH/OH_{sh}^{eq}. Black line shows the border of OH

673 equilibrium according to condition (1). Magenta line shows $< Crit_{OH} >= 0.1$, dotted white line shows

674 $< {Crit_{OH}}^{m} >= 0.1$.

675

676

https://doi.org/10.5194/egusphere-2024-614
Preprint. Discussion started: 5 March 2024

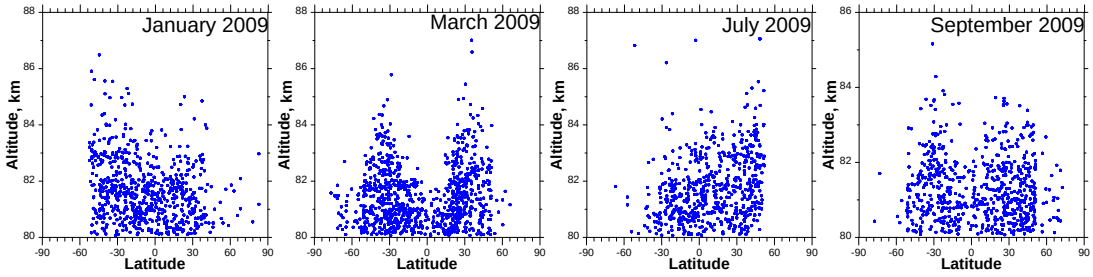

677

678 The Figure 12. Blue dots point the found values of $z_{OH_{sh}^{eq}}$ above 80 km derived from the Panka et al. data

679 in different months of 2009.